EUROPEAN COMMISSION
5th EURATOM FRAMEWORK PROGRAMME 1998-2002
KEY ACTION : NUCLEAR FISSION

HTR-E

High-Temperature Reactor Components and Systems

CONTRACT N°
FIKI-CT-2001-00177

Work Package 2 – Recuperator
Deliverable D-15: Engineering studies – CFD and FEM calculations

J.H. Fokkens

NRG

NETHERLANDS

Dissemination level: CO
Document N° : HTR-E-05/09-D-2-2-3
Status: final
NRG identification number: 20793/05.67283/C

This page is intentionally left blank.

Confidential

HTR-E WP 2

Thermal and Mechanical Analyses for Heatric Mock-Up

J.H. Fokkens
S.M. Willemsen

Petten, 14 September 2005

20793/05.67283/C

Under the contract of the European Commission and the Netherlands Ministry of Economic Affairs

author :	J.H. Fokkens	reviewed :	J.M. Church
59 page(s)		approved :	V.A. Wichers

© NRG 2005

Subject to agreement with the client, the information contained in this report may not be disclosed to any third party and NRG is not liable for any damage arising out of the use of such information.

Acknowledgement

The work reported here is carried out for the 5^{th} Framework programme HTR-E (contract nr. FIKI-CT-2001-00177) with financial support from the European Commission and the Netherlands Ministry of Economic Affairs. The report is a contribution of NRG to HTR-E WP 2.

Contents

List of Tables **4**

List of Figures **4**

1 Introduction **7**

2 Problem Definition **9**

3 Computational Fluid Dynamics Analyses **11**

3.1 Model Description 11

3.1.1 Geometry 11

3.1.2 CFD Model 12

3.1.3 Material Properties 12

3.1.4 Boundary and Loading Conditions 12

3.2 Steady State Results 13

3.3 Results Cool Down Transient 13

4 Mechanical Analyses **15**

4.1 Model Description 15

4.1.1 Approach and FE Model 15

4.1.2 Material Properties 15

4.1.3 Boundary and Loading Conditions 16

4.2 Finite Element Results 16

5 Fatigue Evaluations **17**

5.1 Approach 17

5.2 Results 17

5.3 Sensitivity Analyses 18

6 Conclusions **21**

References **23**

Figures **25**

Appendix A **47**

List of Tables

1	Loading conditions for the steady state CFD calculation	13
2	Applied temperature dependent material properties for AISI 316 L	15
3	Design fatigue endurance limits for AISI 316 L at 510 ^{o}C	17
4	Maximum number of fatigue cycles for the critical positions according to an ASME and RCC-MR fatigue evaluation	18
5	Results sensitivy analysis of fatigue evaluation according to ASME	19
6	Results sensitivy analysis of fatigue evaluation according to RCC-MR	19

List of Figures

1	HTR principle	25
2	A schematic layout of the Heatric mock-up design	26
3	Calculation grid used for the CFD analyses	26
4	Detailed views of the CFD calculation grid	27
5	Cross section view of passages in the Heatric mock-up	27
6	The applied cool down transient for the Claire mock-up in the CFD calculation	28
7	The steady state temperature distribution at the hot and cold side of the mock-up	28
8	The steady state pressure distribution in the gas at the hot and cold side of the mock-up	29
9	The steady state gas velocity distribution at the hot and cold side of the mock-up	29
10	The steady state distribution of the heat flux at the hot and cold side of the mock-up	29
11	The temperature at the hot and cold in- and outlet as a function of time during the cool down transient	30
12	The temperature distribution along cross section A-A at various time intervals during the cool down transient	30
13	The temperature distribution at the hot and cold side of the mock-up after 25 seconds during the cool down transient	31
14	The pressure distribution in the gas at the hot and cold side of the mock-up after 25 seconds during the cool down transient	31
15	The gas velocity distribution at the hot and cold side of the mock-up after 25 seconds during the cool down transient	31
16	The temperature distribution at the hot and cold side of the mock-up after 50 seconds during the cool down transient	32
17	The pressure distribution in the gas at the hot and cold side of the mock-up after 50 seconds during the cool down transient	32
18	The gas velocity distribution at the hot and cold side of the mock-up after 50 seconds during the cool down transient	32
19	The temperature distribution at the hot and cold side of the mock-up after 100 seconds during the cool down transient	33
20	The pressure distribution in the gas at the hot and cold side of the mock-up after 100 seconds during the cool down transient	33
21	The gas velocity distribution at the hot and cold side of the mock-up after 100 seconds during the cool down transient	33

22 The temperature distribution at the hot and cold side of the mock-up after 300 seconds during the cool down transient 34
23 The pressure distribution in the gas at the hot and cold side of the mock-up after 300 seconds during the cool down transient 34
24 The gas velocity distribution at the hot and cold side of the mock-up after 300 seconds during the cool down transient 34
25 The temperature distribution at the hot and cold side of the mock-up after 700 seconds during the cool down transient 35
26 The pressure distribution in the gas at the hot and cold side of the mock-up after 700 seconds during the cool down transient 35
27 The gas velocity distribution at the hot and cold side of the mock-up after 700 seconds during the cool down transient 35
28 The temperature distribution at the hot and cold side of the mock-up after 1500 seconds during the cool down transient 36
29 The pressure distribution in the gas at the hot and cold side of the mock-up after 1500 seconds during the cool down transient 36
30 The gas velocity distribution at the hot and cold side of the mock-up after 1500 seconds during the cool down transient 36
31 The temperature distribution at the hot and cold side of the mock-up after 3600 seconds during the cool down transient 37
32 The pressure distribution in the gas at the hot and cold side of the mock-up after 3600 seconds during the cool down transient 37
33 The gas velocity distribution at the hot and cold side of the mock-up after 3600 seconds during the cool down transient 37
34 The finite element model of the Heatric mock-up 38
35 Detailed view of the finite element model of the Heatric mock-up 38
36 The applied material sets and boundary conditions for the finite element model 39
37 The distribution of the axial displacement after 0 and 700 seconds during the cool down transient 40
38 The distribution of the displacement in thickness direction after 0 and 700 seconds during the cool down transient 40
39 The decrease of axial length of the mock-up as a function of time during the cool down transient 41
40 The decrease of thickness of the mock-up as a function of time during the cool down transient 41
41 The distribution of the Tresca stress in the mock-up after 0 seconds during the cool down transient 42
42 The distribution of the Tresca stress in the mock-up after 25 seconds during the cool down transient 42
43 The distribution of the Tresca stress in the mock-up after 50 seconds during the cool down transient 43
44 The distribution of the Tresca stress in the mock-up after 100 seconds during the cool down transient 43
45 The distribution of the Tresca stress in the mock-up after 300 seconds during the cool down transient 44

46 The distribution of the Tresca stress in the mock-up after 700 seconds during the cool down transient 44
47 The most critical positions with respect to fatigue damage in the Heatric mock-up 45
48 The temperature in the critical positions as a function of time 46
49 The Tresca stress in the critical positions as a function of time 46
A.1 The positions of all thermocouples 47
A.2 The possible positions of the thermocouples T12e up to T20e 47
A.3 The predicted temperature as a function of time for thermocouples T1d untill T6d 48
A.4 The predicted temperature as a function of time for thermocouples T7d_ec untill T11d_ec 49
A.5 The predicted temperature as a function of time for thermocouple T12e at different levels 50
A.6 The predicted temperature as a function of time for thermocouple T13e at different levels 51
A.7 The predicted temperature as a function of time for thermocouple T14e at different levels 52
A.8 The predicted temperature as a function of time for thermocouple T15e at different levels 53
A.9 The predicted temperature as a function of time for thermocouple T16e at different levels 54
A.10 The predicted temperature as a function of time for thermocouple T17e at different levels 55
A.11 The predicted temperature as a function of time for thermocouple T18e at different levels 56
A.12 The predicted temperature as a function of time for thermocouple T19e at different levels 57
A.13 The predicted temperature as a function of time for thermocouple T20e at different levels 58
A.14 The predicted temperature as a function of time for thermocouples T21d untill T25d 59

1 Introduction

This report contributes to the 5^{th} Framework Programme HTR-E WP 2. The aim of HTR-E WP 2 is to give an insight into the behaviour of the recuperator in a direct cycle High Temperature Helium Cooled Reactor design during a thermal transient. From the various recuperator designs available two designs have been chosen to be investigated in detail within the project [1, 2, 3]. One design based on printed circuit technology (Heatric) and one design based on plate fin technology (Nordon) have been chosen. A mock-up of both designs is to be tested in the CLAIRE test loop at CEA Grenoble with a large number of start up and cool down thermal transients.

This report summarizes the results of the thermal and mechanical analyses performed for the Heatric mock-up to be tested in the CLAIRE test loop. The thermal transient behaviour of the mock-up during a cool down transient has been calculated with a computational fluid dynamics (CFD) transient analysis. The stresses in the mock-up during a cool down transient have been calculated with a transient elastic finite element (FEM) analysis. The transient temperatures calculated with the CFD analysis have been used as a thermal loading in the FEM analysis. For the most highly loaded locations of the mock-up fatigue evaluations have been performed. For the fatigue evaluations the stress range during the cool down transient in each location is used as input. Fatigue evaluations have been performed based on the ASME [4] as well as the RCC-MR [5] fatigue data.

2 Problem Definition

The principle of an HTR reactor is shown in Figure 1. The helium gas coming from the high pressure compressor and going to the reactor vessel is heated in the recuperator by the helium gas coming from the turbine and going to the pre-cooler. The use of a recuperator results in a substantial efficiency increase. A recuperator should have a high thermal efficiency, low pressure losses, and a compact design. During a loss of offsite power with a turbo-machine trip the recuperator will endure a cool down and subsequent start up thermal transient. These transients are severe, but the recuperator design should be able to withstand a number (500) of these transients during its operational life [6].

Within the framework of the HTR-E project the behaviour during thermal transients of two recuperator designs is being investigated. The first design is based on printed circuit technology (Heatric) and the other design on plate fin technology (Nordon). A mock-up of both designs has to endure a large number of start up and cool down transients in the Claire test loop at CEA Grenoble. The mock-ups to be tested in the Claire loop operate with air instead of helium and have a reduced size and capacity due to the restrictions imposed by the test loop.

The start up and cool down thermal transients result in large stress changes in the mock-up design. These stress changes result potentially in thermal fatigue damage in the mock-up, which eventually can result in failure of the mock-up. The fatigue behaviour of the Heatric mock-up during a cool down transient has been investigated using numerical simulations. The cool down transient has been chosen, because it is the most severe thermal transient experienced by the recuperator. The fatigue strength of the Heatric recuperator mock-up has been evaluated using a three step approach:

- determination of the transient thermal response of the mock-up;
- determination of the stress changes due to the transient thermal response;
- fatigue life evaluation according to nuclear safety codes based on the stress changes.

The transient thermal response of the recuperator mock-up has been determined using a computational fluid dynamics (CFD) analysis. In a CFD analysis the heat transfer through the mock-up is calculated based on the mass flow and the inlet temperatures of the air flow at the hot and cold side. Incorporated in the CFD analysis of the mock-up is the interaction between the air flows and the solid material. CFD has been chosen for the calculation of the transient thermal response of the mock-up because of the advanced modelling available for the interaction, especially at the interface between gas and solid material.

The cool down transient results in substantial thermal gradients in the mock-up. Especially in the Heatric mock-up, because it has a large thermal capacity due to its solid design. The thermal gradients in the mock-up result in large thermal deformations and stresses. The thermal deformations and stresses in the mock-up have been calculated using a transient Finite Element (FE) analysis. The FE analysis uses the CFD transient thermal results as a thermal load input. The FE results give in each location of the mock-up the stress change during the cool down transient.

Fatigue damage in a structure is caused by a cyclic stress loading. In the mock-up fatigue damage will occur at the locations with large stress changes during the cool down transient. The number of cycles until failure can be calculated by comparing the stress (or strain) amplitude per cycle with the

fatigue endurances curves as given in nuclear safety codes [4, 5]. This approach, using fatigue curves from safety codes, results in very conservative estimates for the number of cycles until fatigue failure, because of the safety margins incorporated in the fatigue curves. This should be kept in mind when viewing the fatigue life predictions for the recuperator mock-up tested in the Claire loop. For the mock-up the fatigue life predictions will be supplemented by evaluations in which the sensitivity of the fatigue life prediction for various load parameters is elucidated.

3 Computational Fluid Dynamics Analyses

The steady state and transient thermal behaviour of the Heatric mock-up has been determined using computational fluid dynamics (CFD) analyses. The CFD analyses have been performed with the general purpose CFD program CFX 5.7 [7]. The geometry of the mock-up has been simplified to a three-dimensional calculation model containing an infinite array of hot and cold plates. With this simplified model both the steady-state thermal behaviour and the thermal behaviour during a cool down transient have been calculated.

3.1 Model Description

3.1.1 Geometry

The Heatric mock-up consists of a stack of plates, in which passages have been etched, through which the air flows. A total of 62 passages have been etched into a single plate. The stack is sealed at the top and the bottom by a plate without passages. The total stack of plates is joined by diffusion bonding, in such a way that the mock-up consists of base material only without metallurgical weaknesses at the plate interfaces. The stack consists of 51 cold side plates and 50 hot side plates. The cold and hot plates are arranged alternately.

Figure 2 shows a schematic layout of the Heatric mock-up. The central part of the mock-up is the fish bone section. Here the passages are etched in a zigzag pattern for optimal heat transfer. In the fish bone section the hot and cold gas flows are operating in counter-flow. The passages in the fish bone section are fed from the feeder channels through the so-called diffusor zone. In this diffusor zone the passages are straight and the hot and cold gas are operating in cross-flow.

With a CFD analysis it is not feasible to make a three-dimensional model of the complete mock-up in which the plates and passages are modelled in detail. A simplified CFD model has to be used to study the thermal behaviour of the mock-up. The following attributes have to be the same in the simplified model as in the actual mock-up:

- the amount of gas flowing through the hot and cold side;
- the total heat transfer between the hot and cold side of mock-up;
- the residence time of the gas flowing through the mock-up;
- the total heat capacity of the solid material in the mock-up.

In the simplified CFD model a single cold and hot plate have been modelled. By choosing an appropriate boundary condition an infinite stack of alternating cold and hot plates has been realised. Notice that in this way the effect of the solid top and bottom plate is neglected. The passages have not been modelled in detail, but the plate volume containing passages has been modelled as a slice of porous material. The porous medium approach requires that in the model the length of the fish bone section is increased in order to obtain the same heat transfer area as in the mock-up. The three-dimensional CFD calculation grid is shown in Figure 3. The grid consists of 132560 cells and 159322 nodes. Detailed views of the calculation grid are shown in Figure 4. The grid has 20 elements in the direction of the thickness, 5 elements for the cold and hot gas flow and 10 for the solid plate in between. The cells size has been chosen in such a way that the gas flow is accurately modelled.

3.1.2 CFD Model

The air flowing through the mock-up has been assumed to be an ideal gas. All air flow is laminar. This implies that the options *non-isothermal*, *single component*, *single phase*, and *laminar* have been activated in CFX 5.7. Also the option that invokes gravity has been activated. The heat transfer in the fluid, the solid, and the fluid-solid interface has been solved simultaneously by CFD code. This so-called *conjugate heat transfer* approach requires no additional boundary conditions for the thermal behaviour.

As already mentioned, the porous medium approach requires an increase in the length of the fish bone section of the model to achieve the same total surface area. The increase in heat capacity due to this increase in length has to be compensated for by adjusting the density of the fish bone section. Figure 5 shows the cross section of the mock-up. The resistance of the porous medium is chosen in such a way that the pressure drop over the mock-up is equal to the pressure drop in PCHE Data Sheet provided by Heatric. The CFX 5.7 option *directional loss model* is utilised to force the gas flow in the direction of the passages by increasing the resistance for flow in the direction perpendicular to the passages.

3.1.3 Material Properties

In the CFD model of the mock-up both the fluid medium (air) and the solid material (stainless steel AISI 316 L) have been modelled. For air the following material properties have been used in the calculations:

density	: ρ =	3.3	[kg / m^3]
viscosity	: η =	2.93E-05	[Pa·s]
thermal conductivity	: λ =	0.06	[W / m·K]
specific heat	: c_p =	1.052E+03	[J / kg·K]

The same air properties have been used as in the PCHE Data Sheet provided by Heatric. These properties have been averaged over the temperature range.

The properties taken for the stainless steel AISI 316 L have been based on the data provided in [8]. The properties used are given below and have been averaged over the temperature range 100 - 500 °C.

density	: ρ =	7907	[kg / m^3]
thermal conductivity	: λ =	18	[W / m·K]
specific heat	: c_p =	532	[J / kg·K]

3.1.4 Boundary and Loading Conditions

For the steady state and transient CFD calculations a standard no-slip boundary condition has been assumed for the walls. Because in practice the mock-up is insulated at the outer boundary in the Claire loop, all outside walls are assumed to be adiabatic. Table 1 summarises the applied loading conditions for the steady-state CFD calculation.
For the transient CFD analysis the hot inlet temperature has been decreased from 510 °C to 105 °C in 5 seconds. The applied cool down transient is illustrated by Figure 6.

table 1 Loading conditions for the steady state CFD calculation

	Cold side	Hot side	
mass flow	0.1	0.1	[kg / s]
inlet temperature	105	510	[^{o}C]
inlet pressure	4.5	4.5	[bar]

3.2 Steady State Results

Steady-state analyses have been used to adjust the CFD model parameters. In particular, the porous material parameters have been adjusted in such a way that a good agreement was reached between the calculated results and the results given by the PCHE Data Sheet provided by Heatric. Figure 7 shows the steady-state temperature distribution in the hot and cold plate side of the mock-up. As expected, the temperatures are much higher at the side where the hot inlet and cold outlet are (right side picture) than at the side where the hot outlet and cold inlet are (left side picture). The difference in temperature between the hot and cold plate side is approximately 10 ^{o}C. Due to the cross flow in the diffusor sections the temperature gradient is different at the top and bottom of the mock-up.

Figure 8 shows the steady-state distribution of the gas pressure at the hot and cold plate side of the mock-up. The steady-state distribution of the gas velocity at the hot and cold plate side of the mock-up is shown in Figure 9. Due to the porous medium approach the calculated velocities in the diffusor sections are slightly increased towards the in- and outlets. However, this is judged to be acceptable. Figure 10 shows the steady-state distribution of the heat flux from the hot to the cold plate. Notice, that this heat flux is not homogeneous over the active length (fish bone section) of the mock-up.

3.3 Results Cool Down Transient

Figure 11 shows the gas temperature as a function of time in the hot and cold in- and outlet. The applied cool down transient has no influence on the gas temperature at the hot outlet due to the large thermal capacity of the mock-up, combined with the very effective heat transfer between the hot and cold plate. The response of the mock-up on the cool down transient can only been seen at the cold outlet. The gas temperature at the cold outlet decreases very rapidly. Because after 1 hour a steady state has nearly been reached in the cold outlet temperature the transient CFD calculation is terminated at this time.

Figure 12 shows the temperature distribution along cross section A-A through the centre of the mock-up (Figure 3) at various time intervals during the cool down transient. At the start of the cool down transient large thermal gradients occur at the side of the mock-up with the hot inlet and cold outlet (right side picture). At the mock-up side with the hot outlet and cold inlet (left side picture) the cool down transient no influence is observed at all. After 1 hour the temperature in the centre of the active part (fish bone section) of the mock-up still exceeds 200 ^{o}C. So, in contrast to what the cold outlet measurement suggests no steady-state temperature distribution has been reached after 1 hour.

In Figures 13 to 33 the distribution of the temperature, gas pressure, and gas velocity at the hot plate and cold plate side of the mock-up are shown at various time intervals during the cool down transient. These figures illustrate that the mock-up does not cool down homogeneously. The mock-up cools down in a longitudinal direction from the end with the hot inlet and cold outlet (right side picture) towards the end with the hot outlet and cold inlet (left side picture). The figures also illustrate the

effect of this cool down behaviour on the pressure distribution and gas velocity.

For the test in the Claire loop thermo-couples have been attached to the mock-up at many positions to measure the temperature as a function of time. For each thermo-couple position as shown in the Figures A.1 and A.2 the calculated temperature as a function of time is given in appendix A, so that after the experiment a comparison can be made between the calculated and measured temperatures.

4 Mechanical Analyses

The deformations and stresses in the mock-up due to the cool down transient have been calculated using a transient finite element (FE) analysis. The FE analysis has been performed with the general purpose program MARC Version 2003 [9]. The FE analysis calculates the stress changes occurring in the mock-up during the cool down transient. The fatigue evaluation is based on these calculated stress changes.

4.1 Model Description

4.1.1 Approach and FE Model

The transient mechanical behaviour of the mock-up has been calculated with an elastic plane stress FE analysis. The transient thermal behaviour calculated with the CFD analysis has been used as the applied loading in the transient mechanical analysis. To simplify the data transfer from the CFD analysis to the FE analysis a similar geometric model has been used. In the FE-model the in- and outlet feeder channels have not been modelled and in the stack direction the model has been reduced to one layer of elements.

Figure 34 shows the utilized FE model. The FE model consists of 10332 elements and 16476 nodal points. The element type used is an eight-node, linear brick element (MARC element type 7). A plane stress analysis can be performed with this three-dimensional model consisting of one layer of elements by applying the correct boundary conditions. Figure 35 shows the mesh distribution around the feeder channels. The sharp corners have been copied from the CFD model. This will result in high peak stresses, which will not occur in the mock-up due to the transition radii at these corners.

4.1.2 Material Properties

The mock-up consists of AISI 316 L. The temperature dependent elastic material properties have been taken from [8]. Table 2 summarizes the material properties utilized for the solid metal. Some parts of the mock-up, as shown in Figure 36, do not consist of solid metal but have a porosity due to the passages running through. For these parts the Young's modulus (E) has been scaled with the porosity. Poisson ratio (ν) and instantaneous coefficient of thermal expansion (λ) have been taken as given in Table 2.

table 2 Applied temperature dependent material properties for AISI 316 L

T [°C]	E [MPa]	ν [-]	λ [1 / °C]
0	200333	0.2921	1.631E-05
50	196273	0.2957	1.670E-05
100	192213	0.2993	1.709E-05
150	188153	0.3029	1.748E-05
200	184093	0.3064	1.787E-05
250	180033	0.3100	1.826E-05
300	175973	0.3136	1.864E-05
350	171913	0.3172	1.902E-05
400	167853	0.3208	1.940E-05
450	163793	0.3244	1.978E-05
500	159733	0.3279	2.016E-05
550	155673	0.3315	2.053E-05

4.1.3 Boundary and Loading Conditions

The FE model contains two planes of nodal points. For all nodes in one plane the displacement perpendicular to the plane has to be suppressed to obtain a plane stress model. Figure 36 shows the postions for which the displacements in the model plane have been suppressed. These boundary conditions simulate the mock-up supports.

The transient temperatures calculated using the CFD analysis have been applied as a thermal load in the FE analysis.

4.2 Finite Element Results

The steady state temperature distribution in the mock-up results in a thermal expansion of the mock-up. This thermal deformation is larger at the hot end of the mock-up than at the cold end. At steady state conditions the thermal elongation of the mock-up is nearly 10 mm and the maximum thickness increase approximately 2.8 mm. During the cool down transient the mock-up the thermal expansion of the mock-up decreases. Figures 37 and 38 show the thermal expansion of the mock-up at steady state conditions and after 700 seconds during the cool down transient. Figure 39 shows the thermal elongation of the mock-up during the cool down transient and Figure 40 the decrease of the thermal expansion in thickness direction.

The rapid cool down of the hot end of the mock-up during the transient results in large thermal gradients and thus high thermal stresses. The Figures 41 to 46 show the distribution of the Tresca stress at various time intervals during the cool down transient. The legend of these figures has been chosen in such a way that the maximum stress corresponds with the yield stress at 510 ^{o}C. The thermal stresses that occur are very high. The figures illustrate in which parts of the mock-up plasticity will occur during a cool down transient. However, the Tresca stresses shown in the figures are elastic stresses. The fatigue evaluation is based on the change of the elastic Tresca stress during the cool down transient.

Large stress changes occur at the interface between the fish bone section and the outside of solid metal near the hot inlet. Figure 47 gives a detailed view of this part of the mock-up. The positions shown in Figure 47 are the most critical positions with respect to fatigue damage. For these positions Figure 48 shows the temperature during the transient as a function of time, while Figure 49 shows the Tresca stress level as a function of time.

5 Fatigue Evaluations

5.1 Approach

Cyclic loading can result in failure of a structure even if the static design criteria are not exceeded. This phenomena is called fatigue failure. When fatigue failure occurs it is determined by the following two factors:

- the amplitude of the applied cyclic load;
- the number of applied cycles.

In nuclear safety codes, such as ASME and RCC-MR, design fatigue endurance curves are given, which describe the relation between the cyclic load amplitude and the number of cycles until the end of the fatigue endurance. Table 3 gives the fatigue design endurance limits for AISI 316 L at 510 ^{o}C as specified in ASME ([4], Table 9.2(a)) and RCC-MR ([5], Table A3.3S.541). In the RCC-MR code the fatigue design endurance limits are given as strain amplitudes versus the number of cycles until the end of the fatigue endurance. The strain amplitudes have been converted to stress amplitudes by using Hooke's law.

table 3 Design fatigue endurance limits for AISI 316 L at 510 ^{o}C

Number of cycles	Allowable stress amplitude	
	ASME	RCC-MR
10	1228.0 MPa	1122.0 MPa
20	699.1 MPa	645.2 MPa
40	457.1 MPa	435.4 MPa
100	318.5 MPa	297.8 MPa
200	251.0 MPa	235.8 MPa
400	215.1 MPa	200.1 MPa
1000	177.2 MPa	163.7 MPa
2000	155.1 MPa	141.6 MPa
4000	137.2 MPa	125.2 MPa
10000	116.5 MPa	106.5 MPa
20000	104.1 MPa	94.9 MPa
40000	95.1 MPa	85.8 MPa
100000	80.7 MPa	72.6 MPa
200000	71.7 MPa	64.9 MPa
400000	64.1 MPa	58.3 MPa
1000000	55.2 MPa	50.4 MPa

5.2 Results

Fatigue failure will occur first at the positions of the mock-up, which are exposed to the largest stress changes during the cool down transients. Large stress changes occur at the interface between the fish bone section and the outside of solid metal near the hot inlet. For the critical positions shown in Figure 47 a fatigue evaluation has been performed. Figure 49 shows the stress change in the critical positions during the cool down transient. A cool-down will result in mainly tensile stresses near the hot inlet, while a start up will result in mainly compressive stresses. The stress levels during a a cool down and a start up transient will be of the same order of magnitude. Therefore, the stress changes, shown in Figure 49, are assumed to be stress amplitudes and a cool down and subsequent start up transient can assumed to be one fatigue cycle.

table 4 Maximum number of fatigue cycles for the critical positions according to an ASME and RCC-MR fatigue evaluation

Position	σ_{amp}	N_{ASME}	$N_{\mathrm{RCC-MR}}$
A	*1024.4 MPa*	*11 cycles*	*11 cycles*
B	*461.4 MPa*	*32 cycles*	*36 cycles*
C	308.3 MPa	80 cycles	92 cycles
D	218.7 MPa	216 cycles	274 cycles
E	231.9 MPa	177 cycles	214 cycles
F	*242.7 MPa*	*155 cycles*	*183 cycles*
G	230.2 MPa	181 cycles	221 cycles
H	194.4 MPa	367 cycles	456 cycles
I	164.4 MPa	806 cycles	980 cycles
J	137.5 MPa	2002 cycles	2360 cycles

Table 4 shows for the critical positions the maximum number of cycles until the end of the fatigue endurance based on fatigue evaluations using the ASME and RCC-MR fatigue design limits. For the positions A, B, and F these results should be viewed with caution. These position are located at geometric discontinuities, which are not modelled in detail. The stress amplitudes calculated are conservative and also the fatigue endurance determined with these stress amplitudes.

The maximum number of fatigue cycles based on the ASME fatigue design limits is slightly more conservative than the maximum number of fatigue cycles based on the RCC-MR fatigue design limits. This is in contrast with the data given in Table 3. For the fatigue evaluation according to the RCC-MR code the stress amplitudes given in Table 4 have been used as input. But for the fatigue evaluation according to the ASME code these stress amplitudee have to be increased with a factor 1.13. This is the ratio between the Young's modulus at 510 $^{\mathrm{o}}$C and the Young's modulus used in the ASME to convert strain amplitudes to stress amplitudes. This approach makes the ASME code more conservative than the RCC-MR code with respect to a fatigue evaluation.

The fatigue endurance predictions based on the fatigue design limits from nuclear safety codes are conservative. These are the minimum number of cycles the structure can withstand and not the number of cycles until failure. A typical safety factor incorporated in the fatigue design limits is a factor of 2 on the stress amplitude. This safety factor on the stress amplitude results in a safety factor of approximately 20 on the number of cycles, due to the logarithmic relation between stress amplitude and number of cycles. For the Claire loop mock-up this should be kept in mind, when viewing the results presented in Table 4. Based on this fact and the results presented here it can be concluded that fatigue failure of the mock-up may not occur during the Claire loop experiment given the planned number of actual cycles.

5.3 Sensitivity Analyses

In support of the Claire loop experiment the influence of a change of the cool down transient on the predicted maximum number of fatigue cycles has been investigated. Three additional cool down transients have been investigated, 510/175, 510/85, and 530/105 $^{\mathrm{o}}$C. It has been assumed that for these transients the stress changes can be determined by scaling the calculated results for the 510/105 $^{\mathrm{o}}$C cool down transient. The scaling factor is the ratio of the temperature differences.

table 5 Results sensitivy analysis of fatigue evaluation according to ASME

Position	510 / 105	510 / 175	510 / 85	530 / 105
A	*11 cycles*	*14 cycles*	*10 cycles*	*7 cycles*
B	*32 cycles*	*47 cycles*	*30 cycles*	*17 cycles*
C	80 cycles	135 cycles	71 cycles	34 cycles
D	216 cycles	513 cycles	183 cycles	71 cycles
E	177 cycles	399 cycles	146 cycles	62 cycles
F	*155 cycles*	*317 cycles*	*135 cycles*	*56 cycles*
G	181 cycles	403 cycles	157 cycles	63 cycles
H	367 cycles	896 cycles	295 cycles	93 cycles
I	806 cycles	2130 cycles	643 cycles	157 cycles
J	2002 cycles	5839 cycles	1557 cycles	333 cycles

Table 5 shows the results of the sensitivity analysis for the fatigue evaluation based on the ASME fatigue design limits, while the results for the fatigue evaluation based on the RCC-MR fatigue design limits are given in Table 6. Both tables show the same tendencies. Reducing the temperature difference of the cool down transient will increase the fatigue endurance, while a larger temperature difference will result in a smaller fatigue endurance. Increasing the maximum temperature will amplify this effect. However, the conclusion that fatigue failure of the mock-up may not occur during the Claire loop experiment remains.

table 6 Results sensitivy analysis of fatigue evaluation according to RCC-MR

Position	510 / 105	510 / 175	510 / 85	530 / 105
A	*11 cycles*	*14 cycles*	*10 cycles*	*7 cycles*
B	*36 cycles*	*55 cycles*	*33 cycles*	*19 cycles*
C	92 cycles	158 cycles	81 cycles	36 cycles
D	274 cycles	633 cycles	224 cycles	81 cycles
E	214 cycles	485 cycles	182 cycles	70 cycles
F	*183 cycles*	*394 cycles*	*159 cycles*	*63 cycles*
G	221 cycles	501 cycles	186 cycles	71 cycles
H	456 cycles	1088 cycles	368 cycles	108 cycles
I	980 cycles	2511 cycles	787 cycles	177 cycles
J	2360 cycles	6902 cycles	1827 cycles	388 cycles

6 Conclusions

Based on the results of the transient thermal and mechanical calculation and the performed fatigue evaluations the following can be concluded for the Heatric mock-up to be tested in the Claire loop:

- The heat transfer through the mock-up is not homogeneous at steady state conditions.
- The mock-up does not cool down homogeneously during the cool down transient. The mock-up cools from the hot end towards the cold end.
- The hot end of the mock-up, where the hot inlet and cold outlet are situated, is exposed to severe thermal transients.
- The complete cool down of the Heatric mock-up takes more than 1 hour.
- At the hot end of the mock-up large stress changes occur during the cool down transient.
- Fatigue failure is most likely to occur at the interface between the fish bone section and the outside solid metal at the hot end of the mock-up.
- Fatigue failure of the Heatric mock-up may not occur during the Claire loop experiment.

It should also be remarked that the fatigue evaluations based on the fatigue design limits given in the ASME and RCC-MR do not predict the number of fatigue cycles until failure of the mock-up. When viewing the results of the performed fatigue evaluations this should be kept in mind. The objective of safety codes is predicting safe operation and not predicting failure.

References

[1] F. Pra (CEA). *HTR-E WP2 Recuperator - Technical Survey*. Document N^{O}: HTR-E-03/01-D-2-2-1; November 2002.

[2] C. Mauget (Framatome ANP). *HTR-E WP2 Recuperator - Consultation of manufacturers*. Document N^{O}: HTR-E-03/06-D-2-2-2-1; June 2003.

[3] C. Mauget (Framatome ANP). *HTR-E WP2 Recuperator - Selection of reference concepts*. Document N^{O}: HTR-E-03/12-D-2-2-4; January 2004.

[4] *ASME Boiler & Pressure Vessel Code, Code Cases, Nuclear Components, Code Case N-204-1*. The American Society of Mechanical Engineers, New York, 1995 Edition, July 1, 1995.

[5] *RCC-MR-Edition 2002, Volume Z.* AFCEN n^{o} 93-2002.

[6] C. Mauget (Framatome ANP). *HTR-E WP2 Recuperator - Specifications of typical operating conditions for HTR.* Document N^{O}: HTR-E-02/08-D-2-1-0; June 2003.

[7] *CFX 5.7 User Guide*. Computational Fluid Dynamics Services, ANSYS, Harwell laboratory, Oxfordshire, UK, 2004.

[8] J.H. Fokkens (NRG). *HTR-E WP2 Recuperator - Material Parameters AISI 316 L*. NRG report 20793/03.56560/C Revision 1; Document N^{O}: HTR-E-04/07-D-2-2-3-1; 30 July 2004.

[9] *MARC2003 Users Manuals*. MSC Software Inc.

Figures

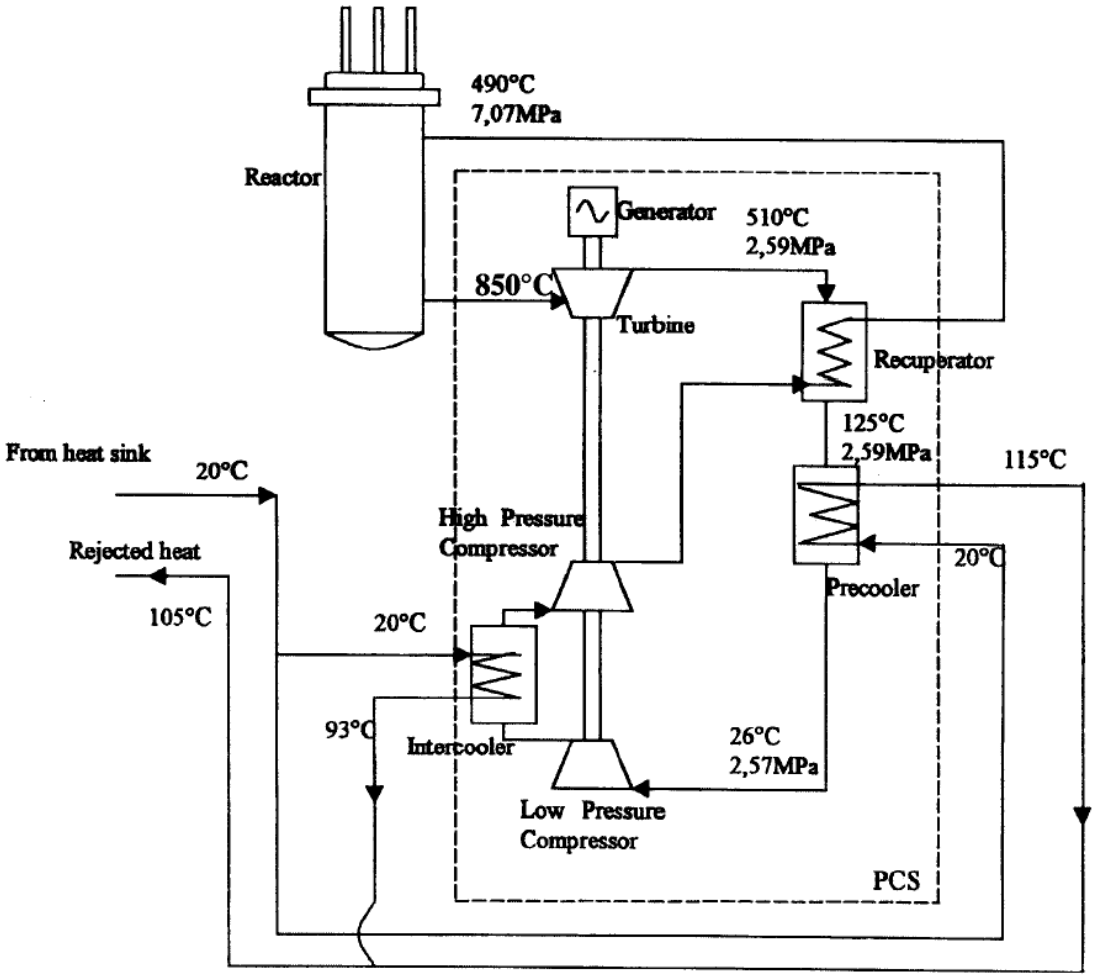


figure 1 HTR principle

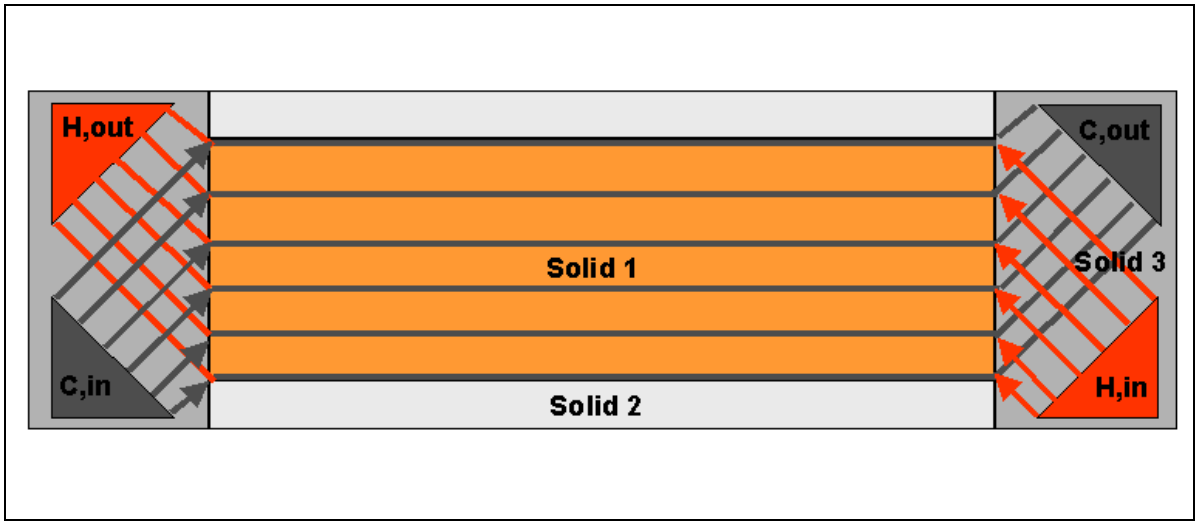


figure 2 A schematic layout of the Heatric mock-up design

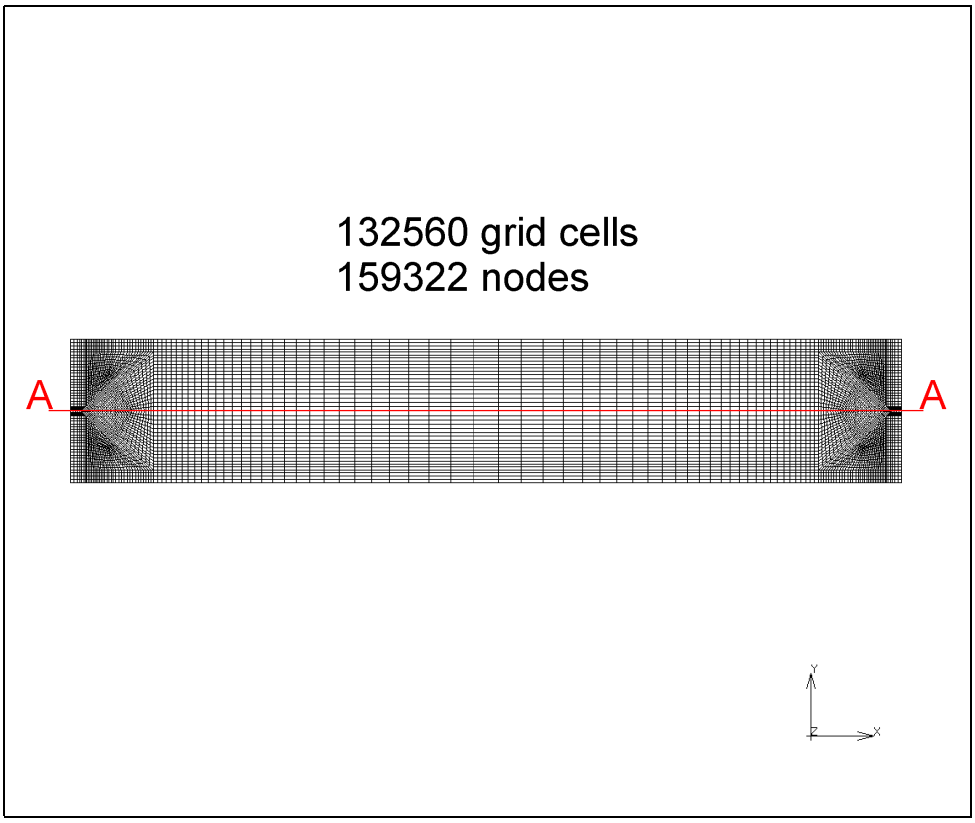


figure 3 Calculation grid used for the CFD analyses

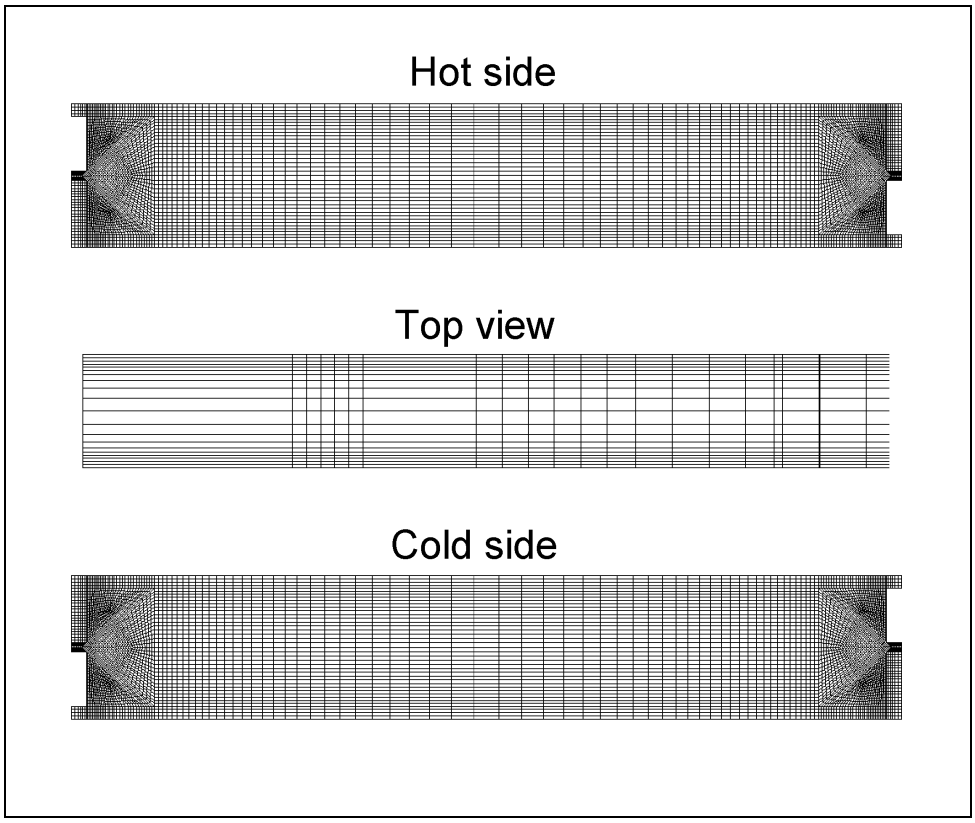


figure 4 Detailed views of the CFD calculation grid

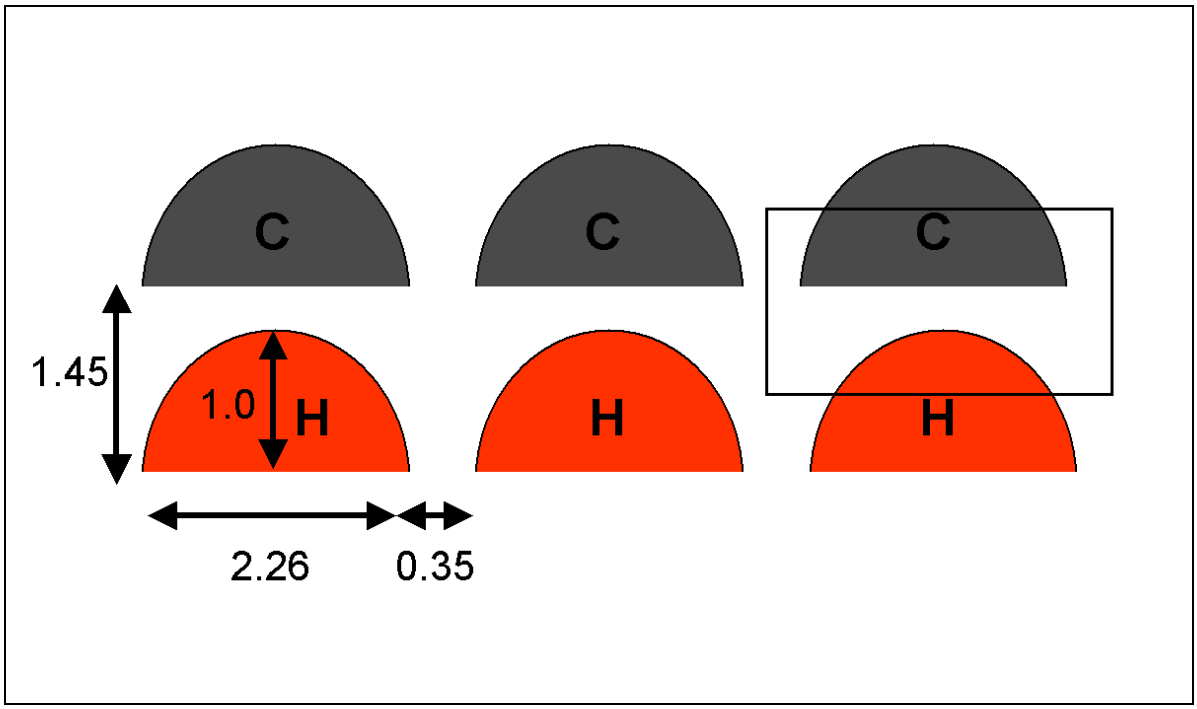


figure 5 Cross section view of passages in the Heatric mock-up

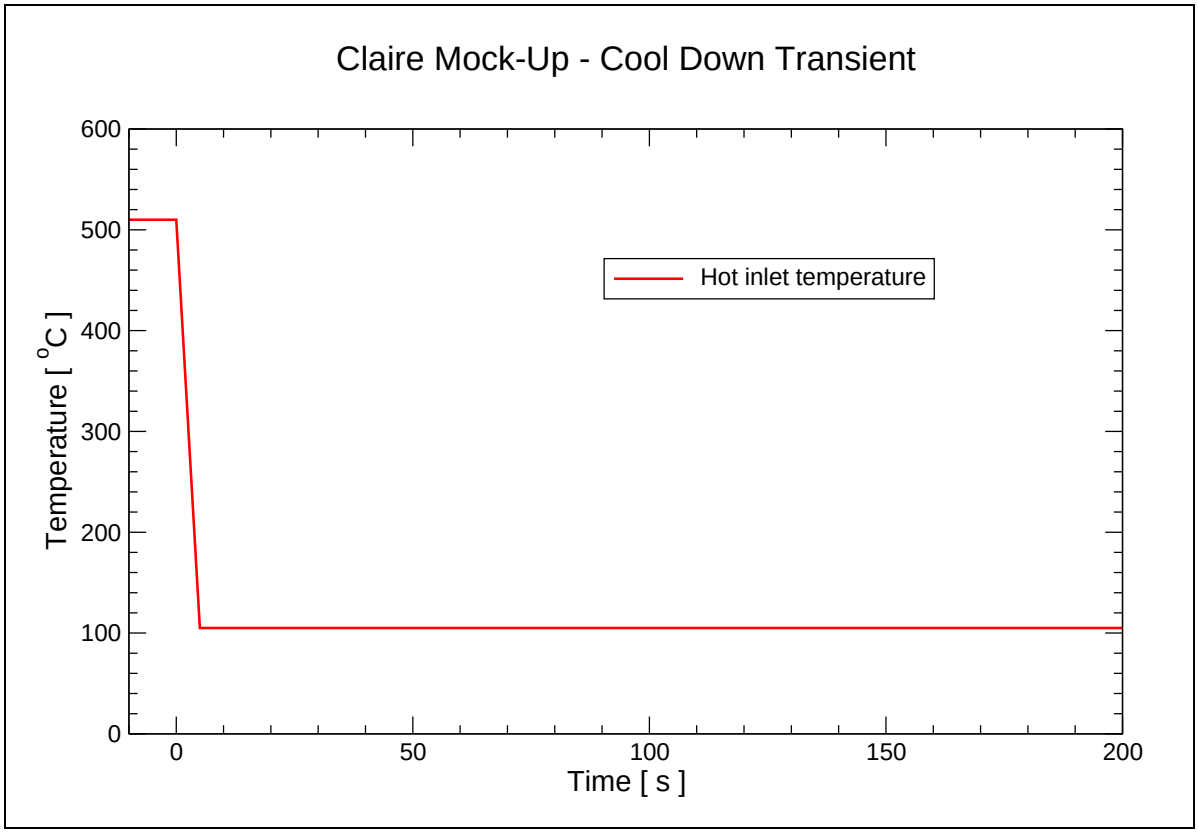


figure 6 The applied cool down transient for the Claire mock-up in the CFD calculation

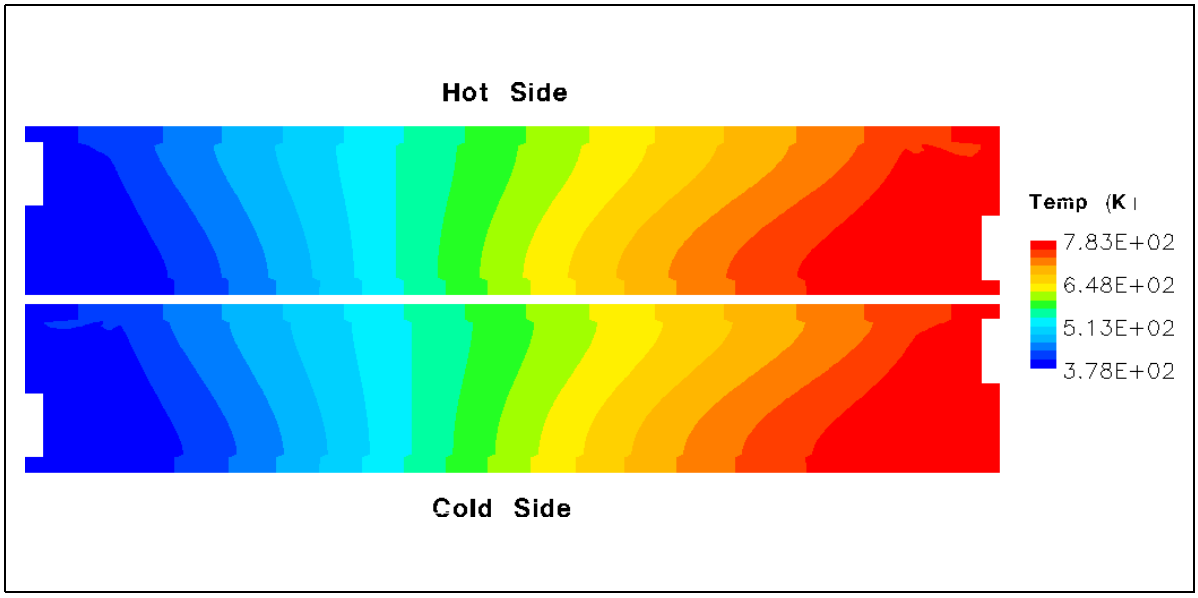


figure 7 The steady state temperature distribution at the hot and cold side of the mock-up

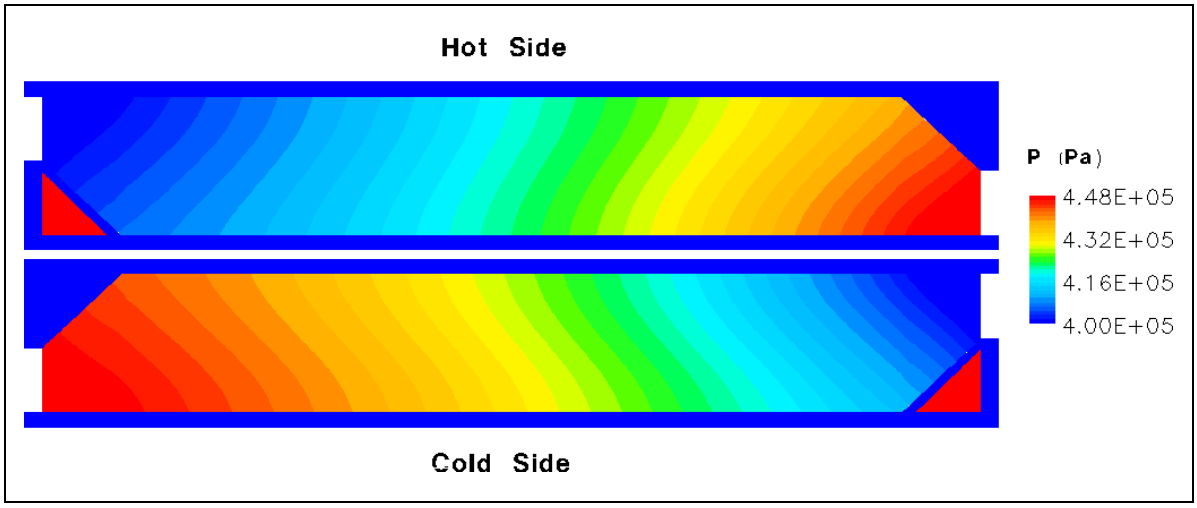


figure 8 The steady state pressure distribution in the gas at the hot and cold side of the mock-up

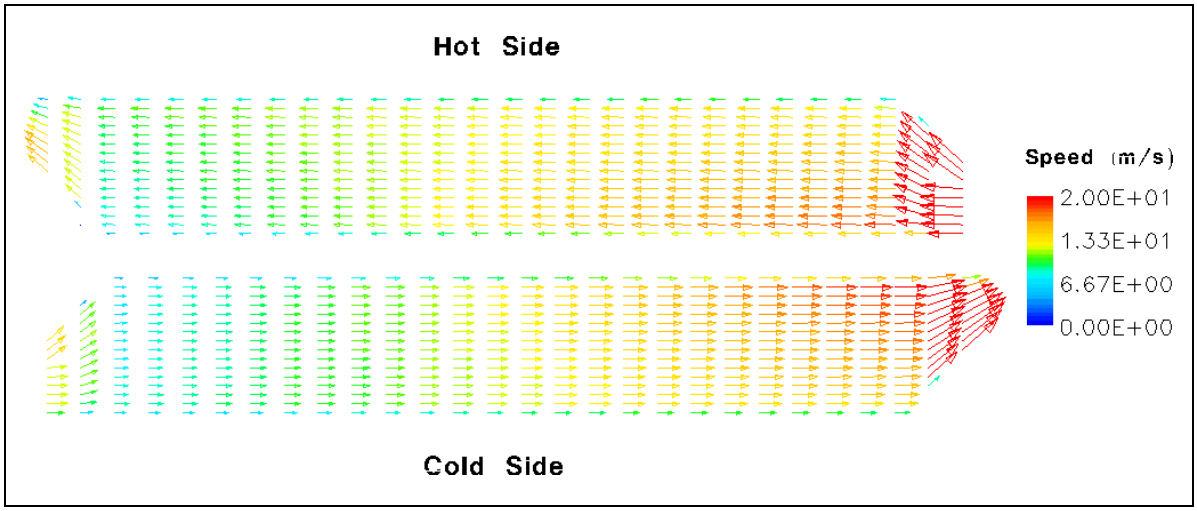


figure 9 The steady state gas velocity distribution at the hot and cold side of the mock-up

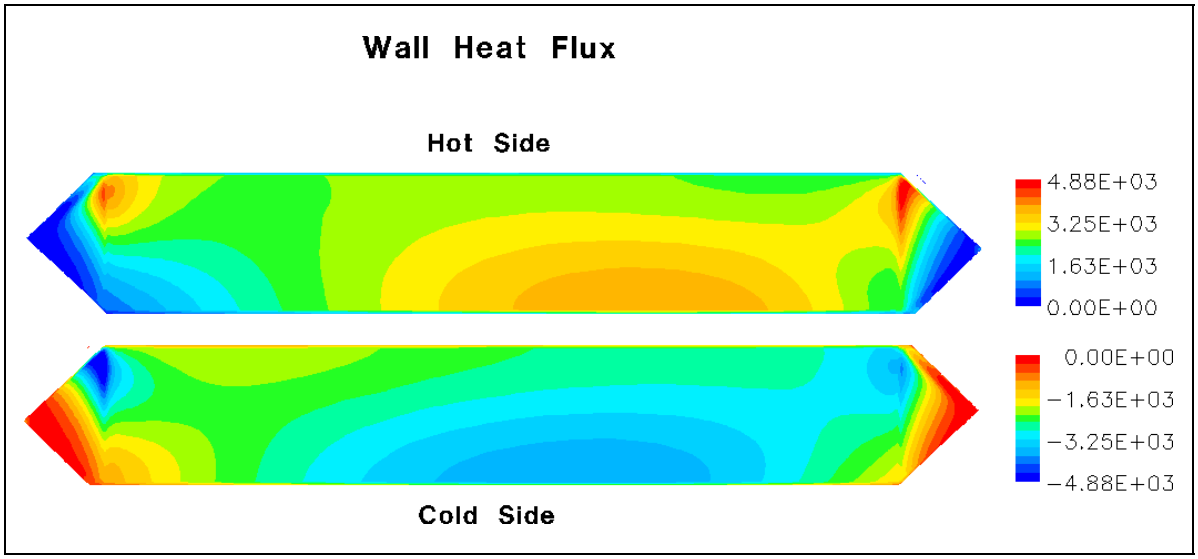


figure 10 The steady state distribution of the heat flux at the hot and cold side of the mock-up

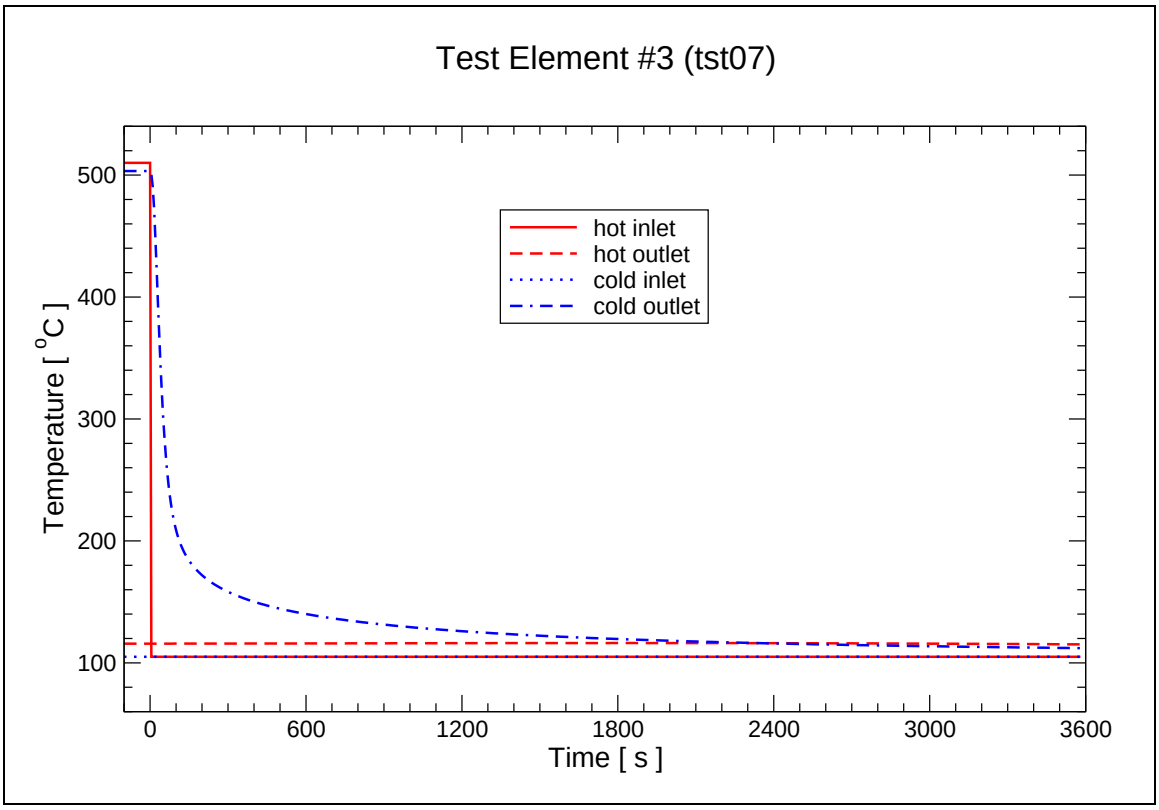


figure 11 The temperature at the hot and cold in- and outlet as a function of time during the cool down transient

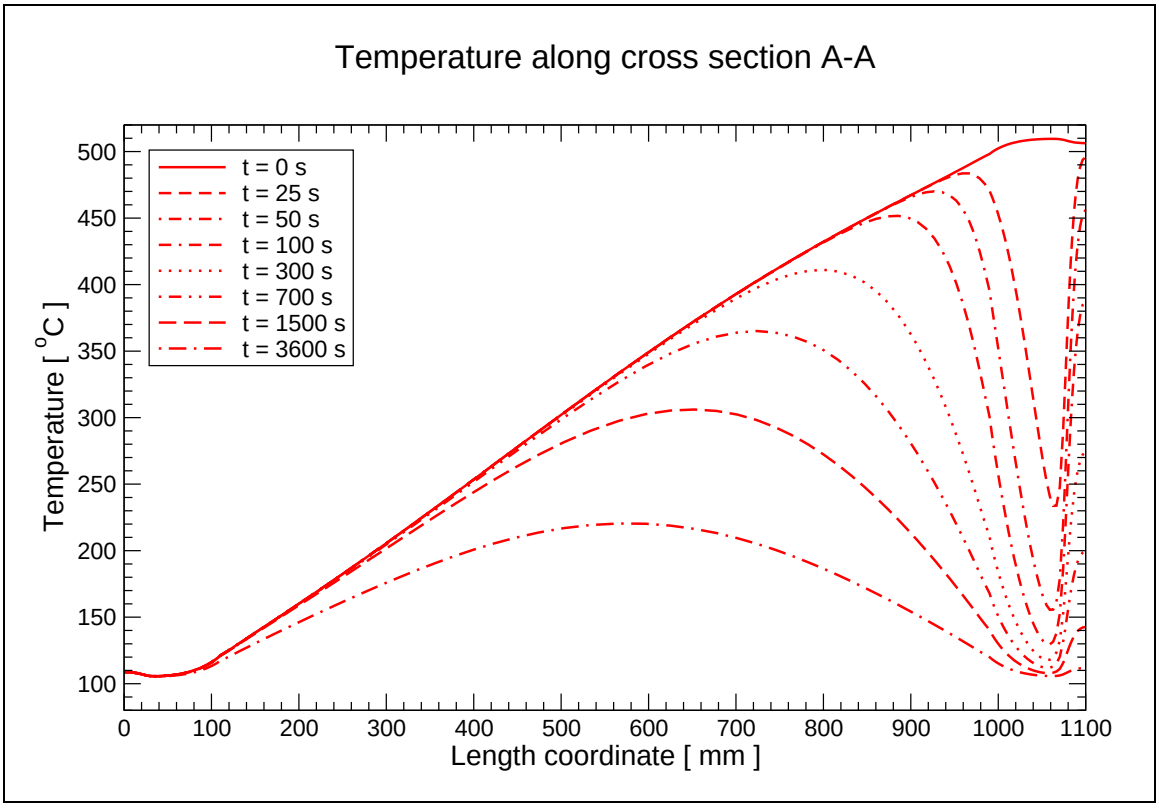


figure 12 The temperature distribution along cross section A-A at various time intervals during the cool down transient

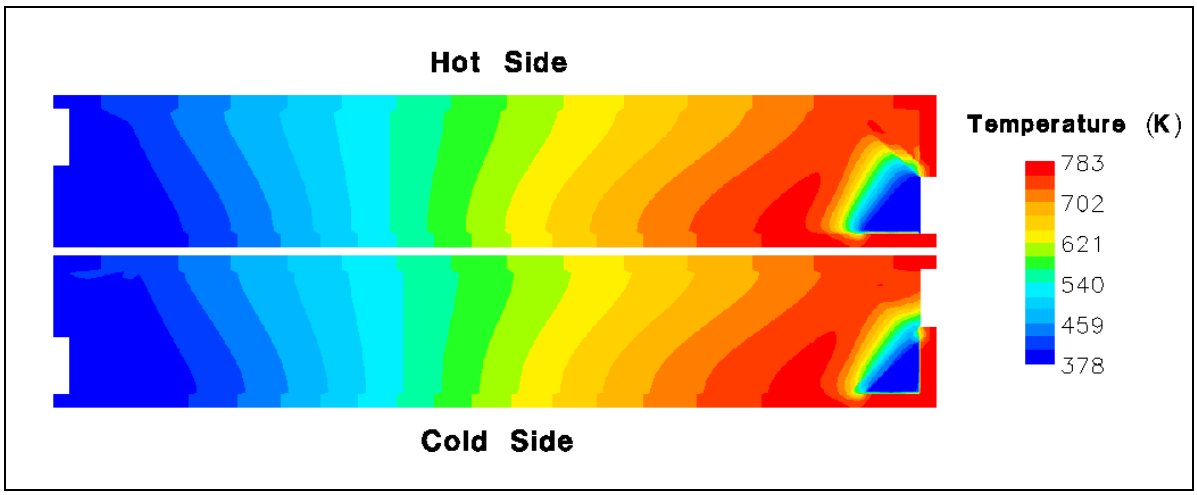


figure 13 The temperature distribution at the hot and cold side of the mock-up after 25 seconds during the cool down transient

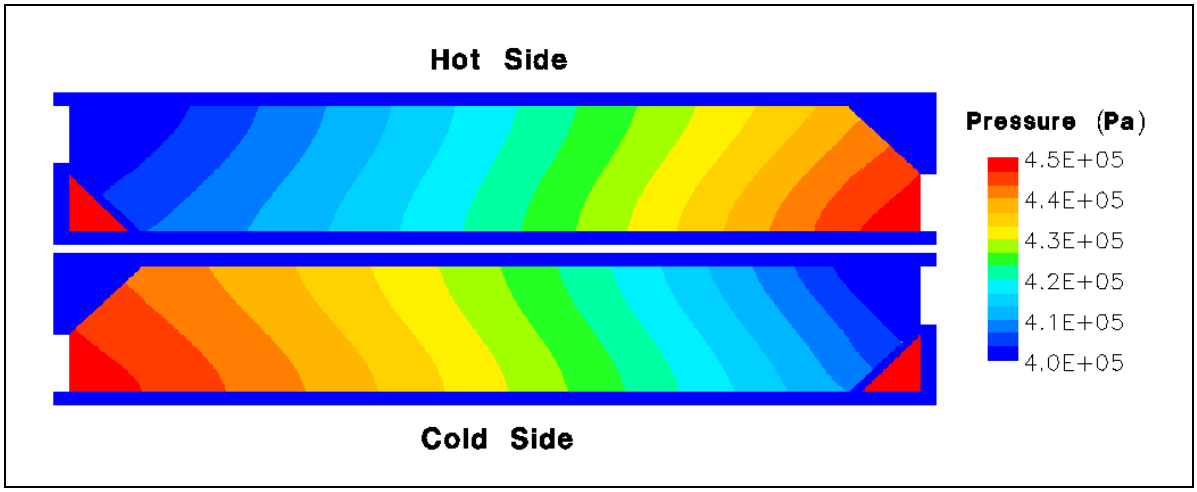


figure 14 The pressure distribution in the gas at the hot and cold side of the mock-up after 25 seconds during the cool down transient

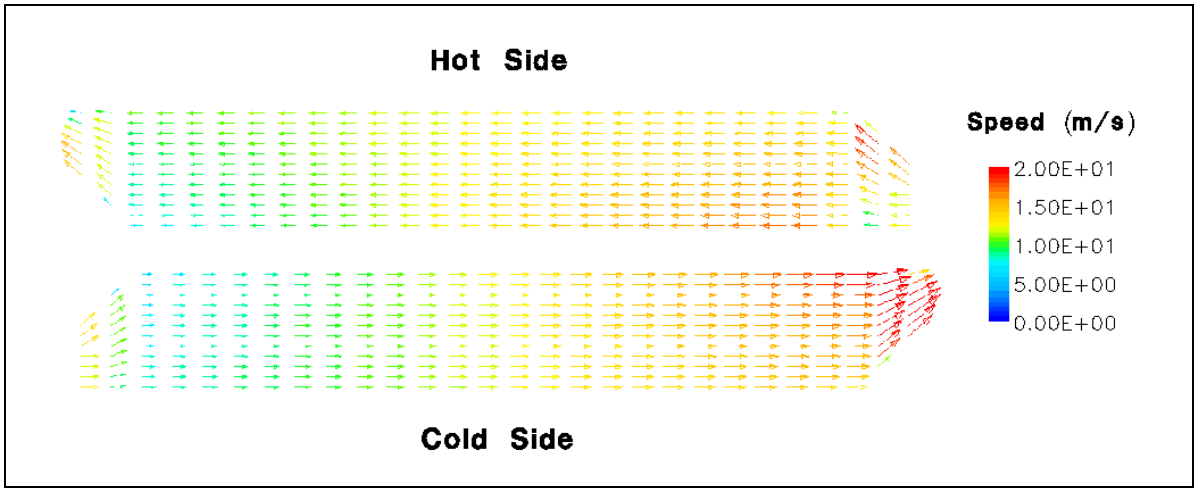


figure 15 The gas velocity distribution at the hot and cold side of the mock-up after 25 seconds during the cool down transient

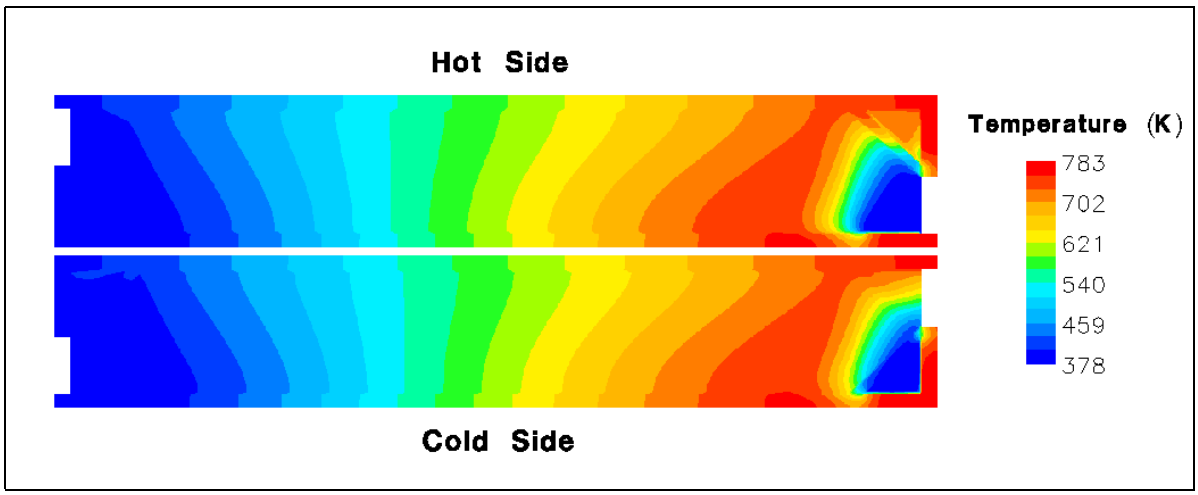


figure 16 The temperature distribution at the hot and cold side of the mock-up after 50 seconds during the cool down transient

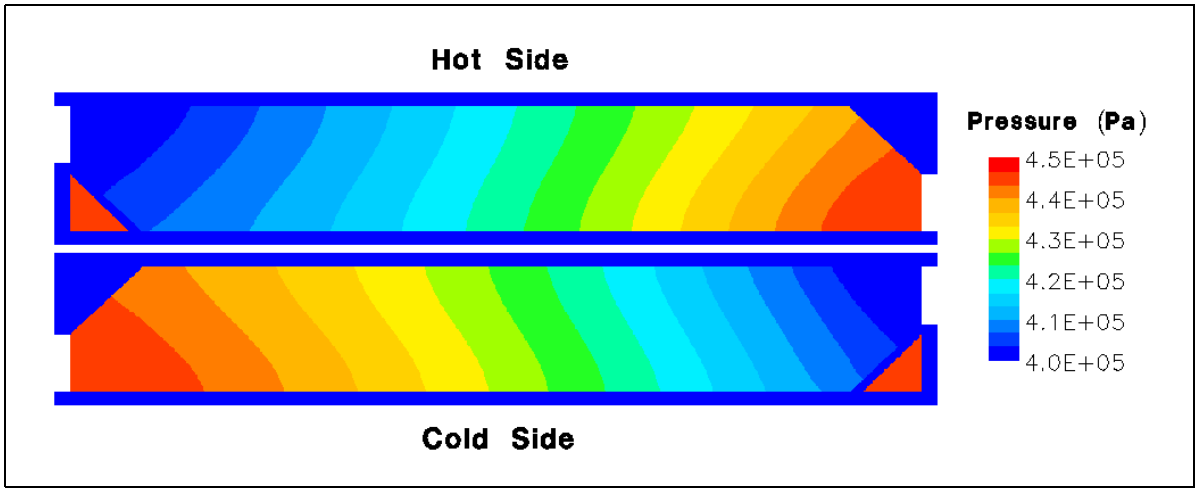


figure 17 The pressure distribution in the gas at the hot and cold side of the mock-up after 50 seconds during the cool down transient

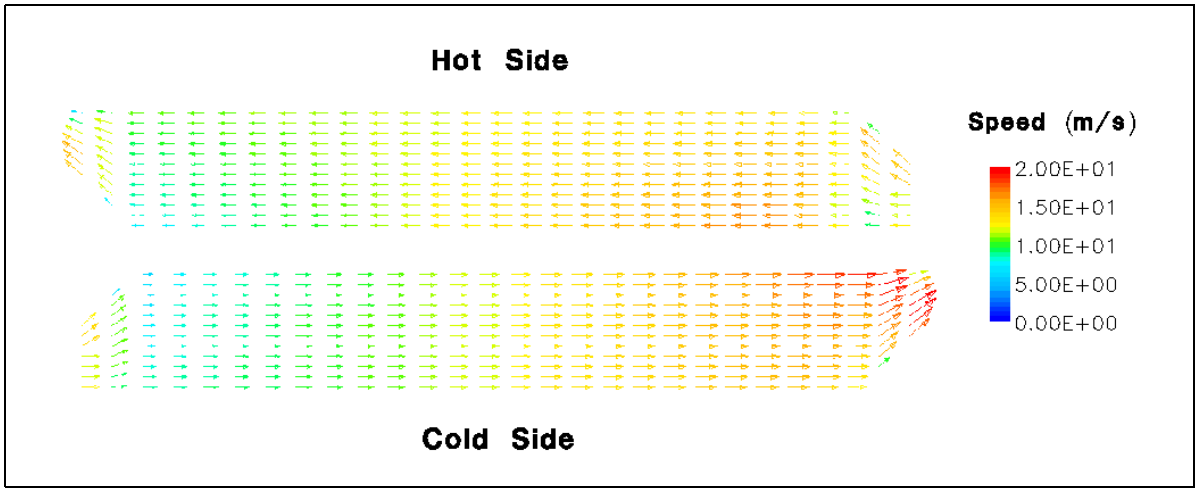


figure 18 The gas velocity distribution at the hot and cold side of the mock-up after 50 seconds during the cool down transient

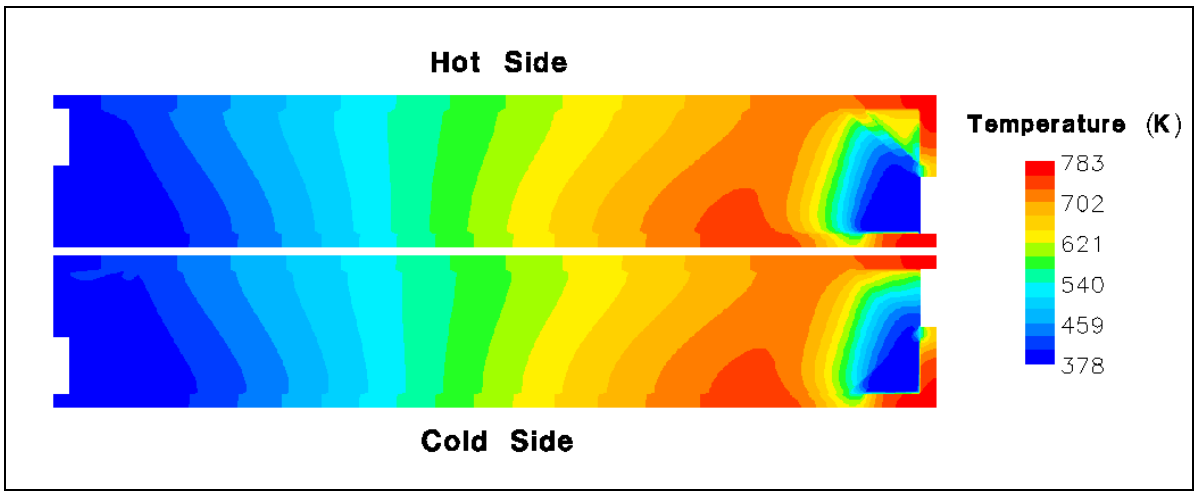


figure 19 The temperature distribution at the hot and cold side of the mock-up after 100 seconds during the cool down transient

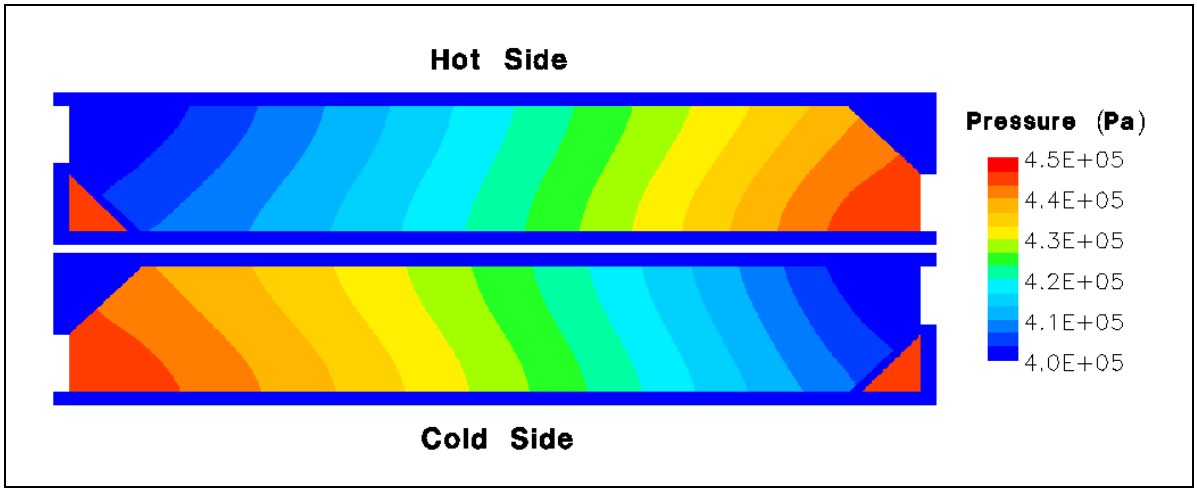


figure 20 The pressure distribution in the gas at the hot and cold side of the mock-up after 100 seconds during the cool down transient

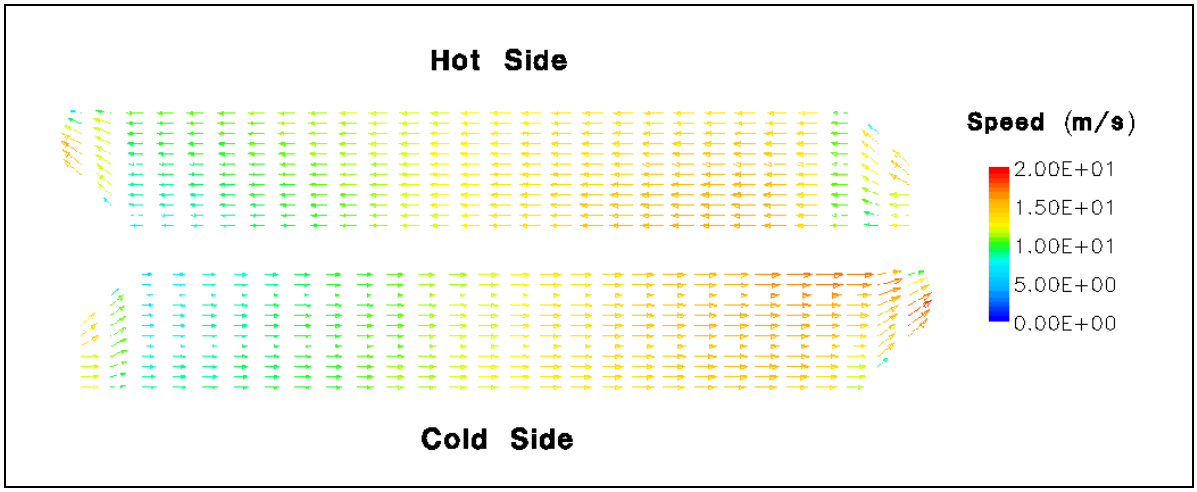


figure 21 The gas velocity distribution at the hot and cold side of the mock-up after 100 seconds during the cool down transient

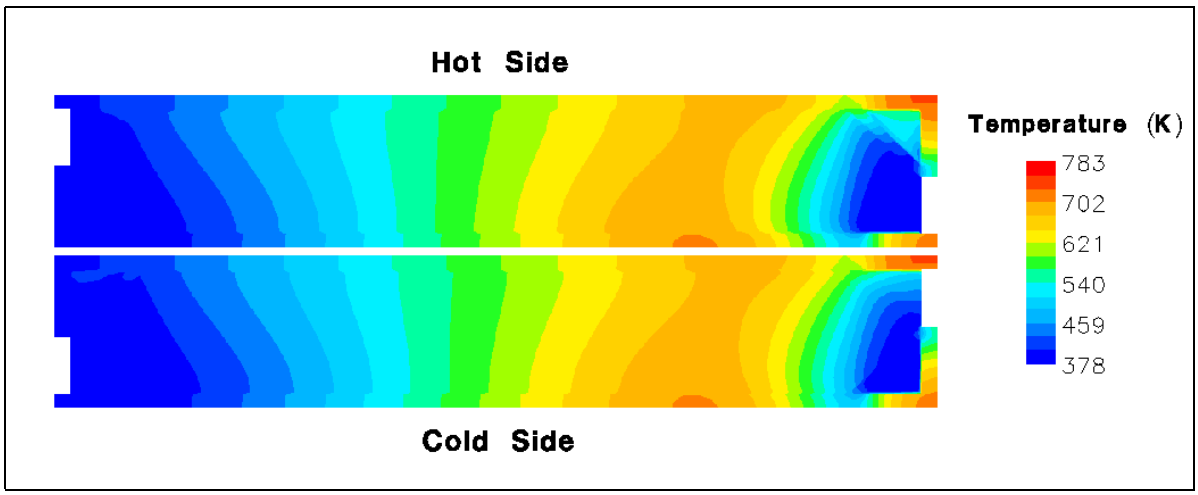


figure 22 The temperature distribution at the hot and cold side of the mock-up after 300 seconds during the cool down transient

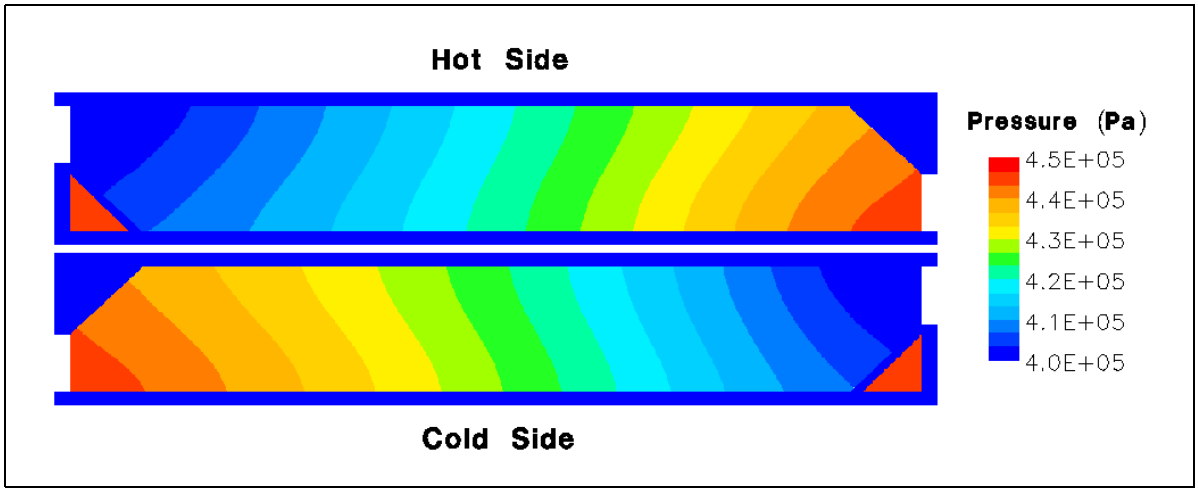


figure 23 The pressure distribution in the gas at the hot and cold side of the mock-up after 300 seconds during the cool down transient

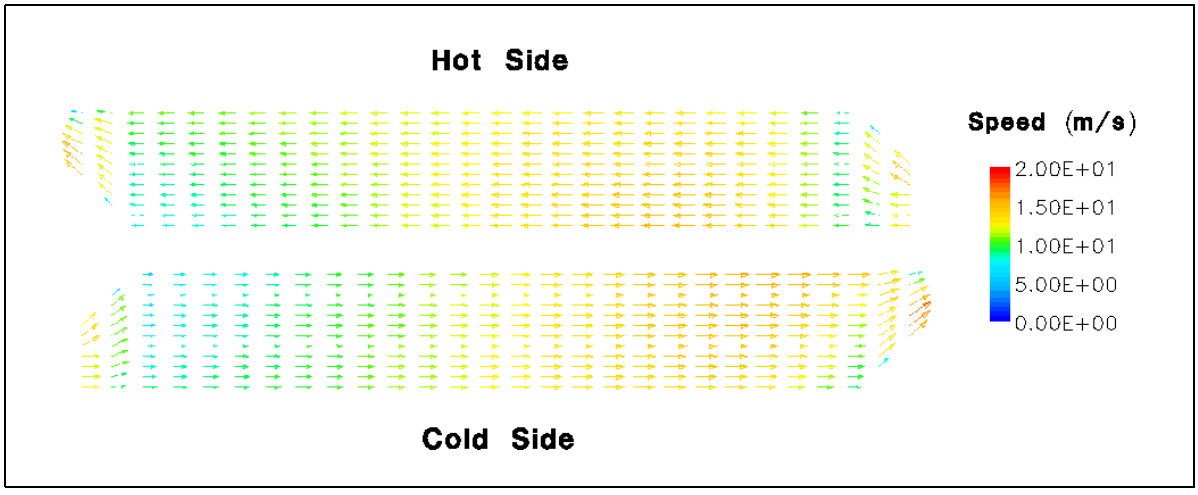


figure 24 The gas velocity distribution at the hot and cold side of the mock-up after 300 seconds during the cool down transient

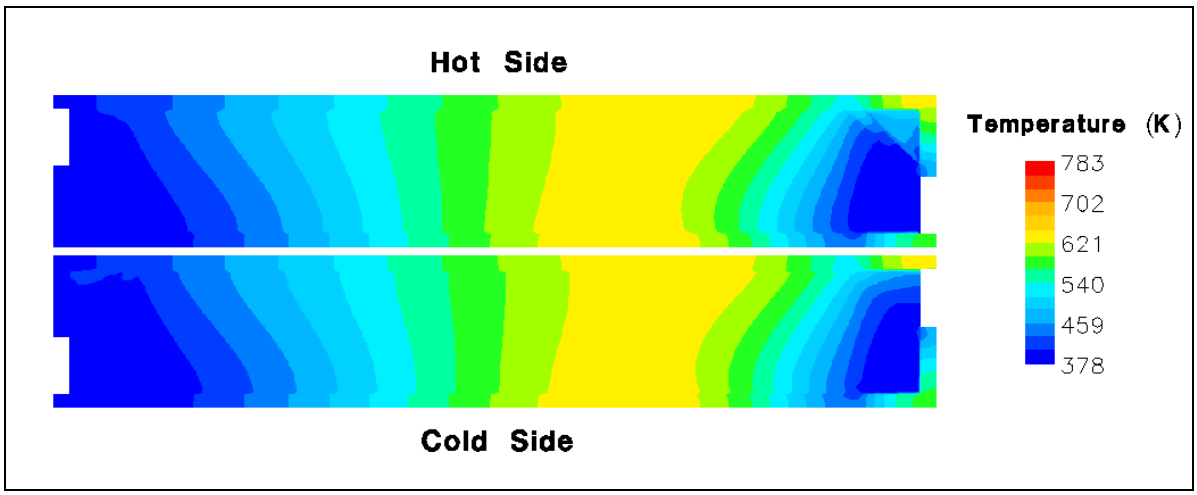


figure 25 The temperature distribution at the hot and cold side of the mock-up after 700 seconds during the cool down transient

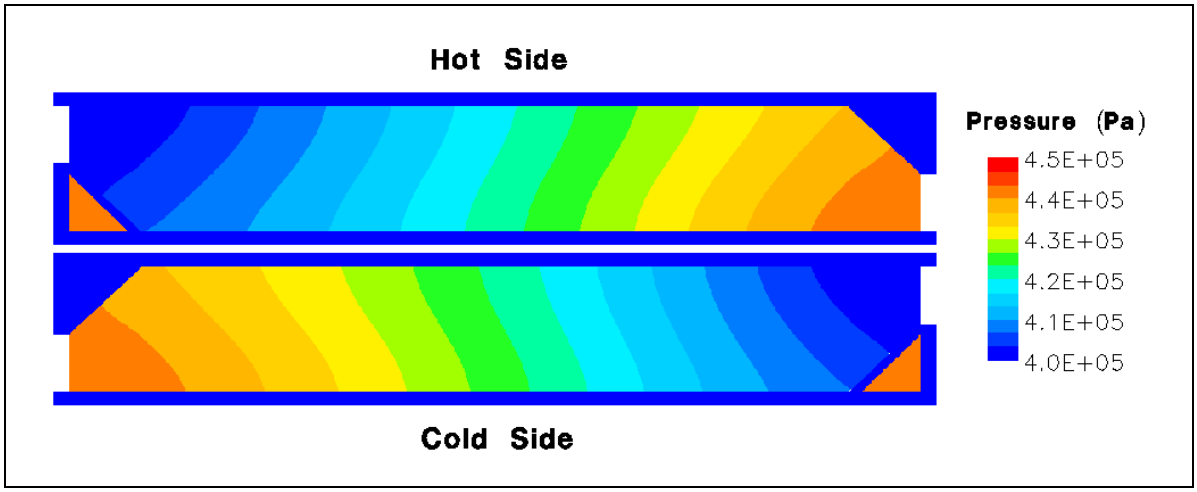


figure 26 The pressure distribution in the gas at the hot and cold side of the mock-up after 700 seconds during the cool down transient

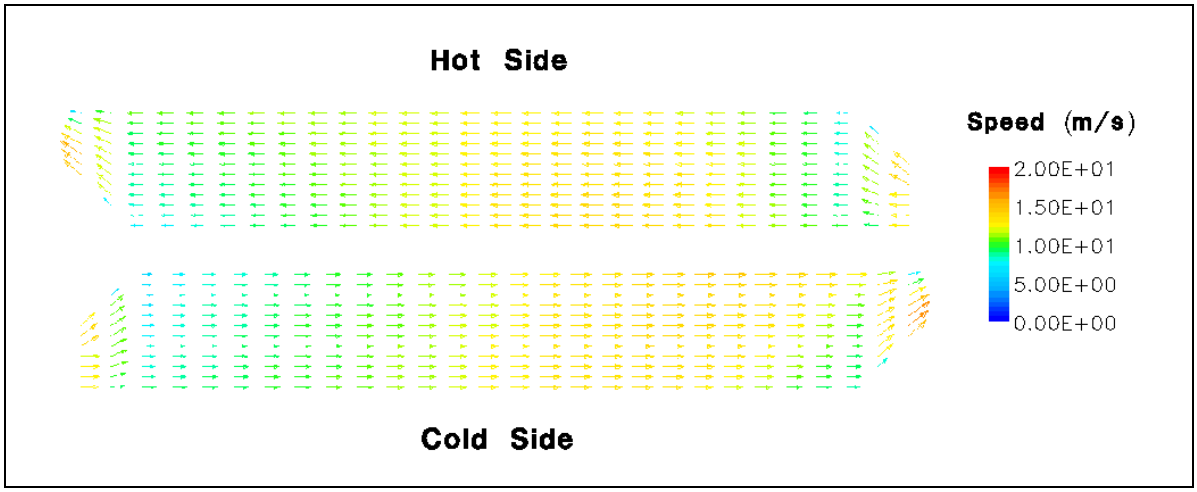


figure 27 The gas velocity distribution at the hot and cold side of the mock-up after 700 seconds during the cool down transient

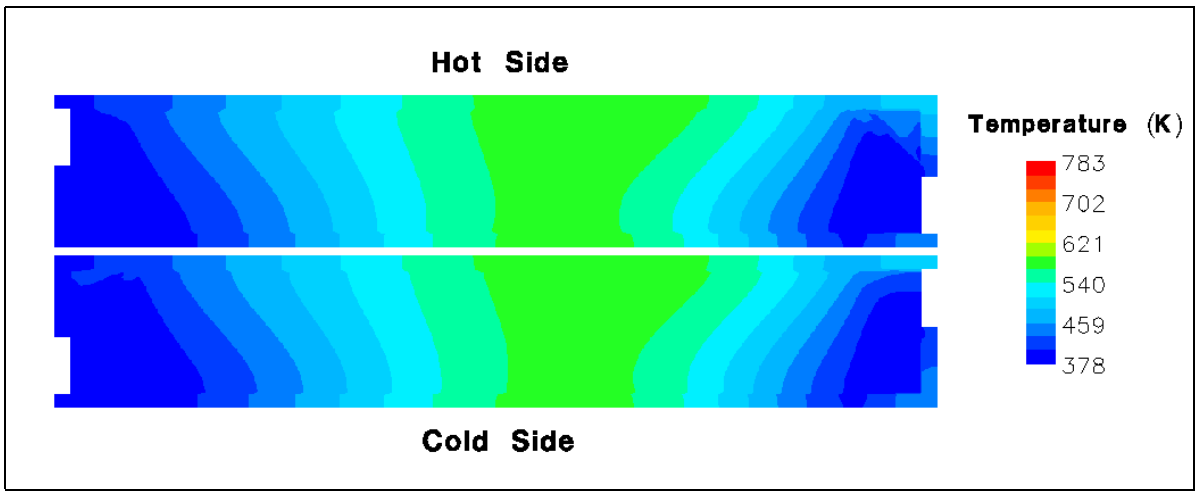


figure 28 The temperature distribution at the hot and cold side of the mock-up after 1500 seconds during the cool down transient

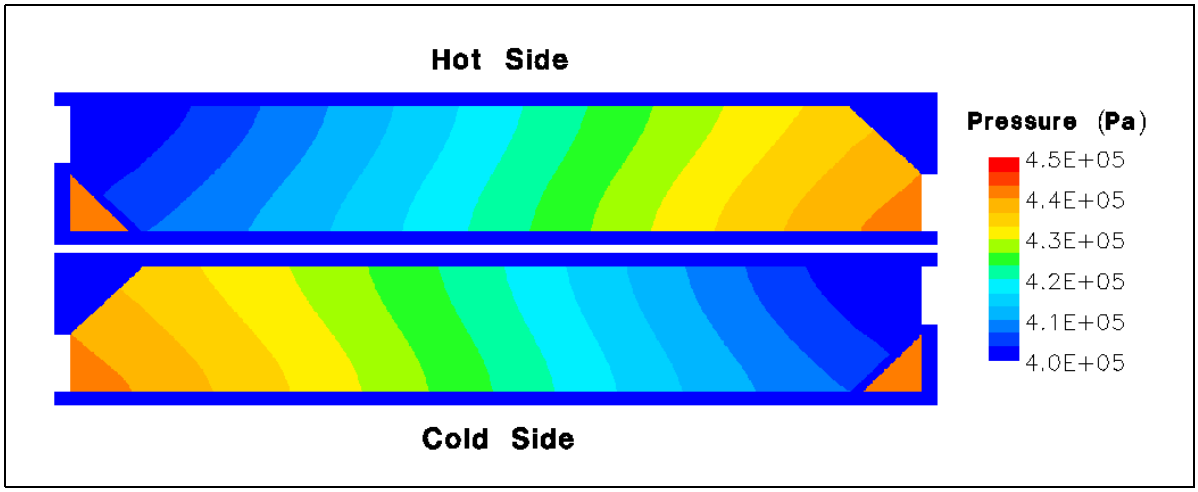


figure 29 The pressure distribution in the gas at the hot and cold side of the mock-up after 1500 seconds during the cool down transient

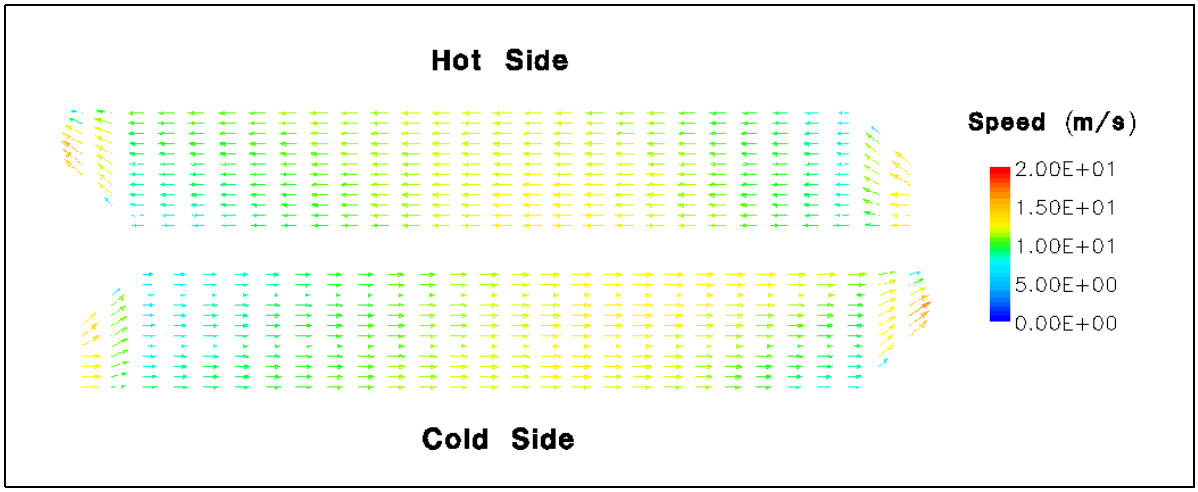


figure 30 The gas velocity distribution at the hot and cold side of the mock-up after 1500 seconds during the cool down transient

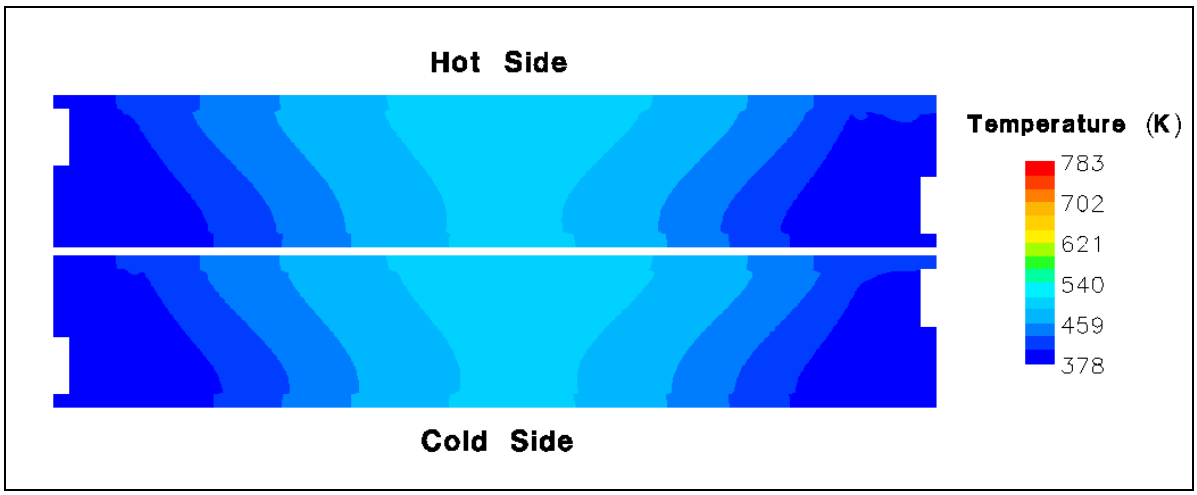


figure 31 The temperature distribution at the hot and cold side of the mock-up after 3600 seconds during the cool down transient

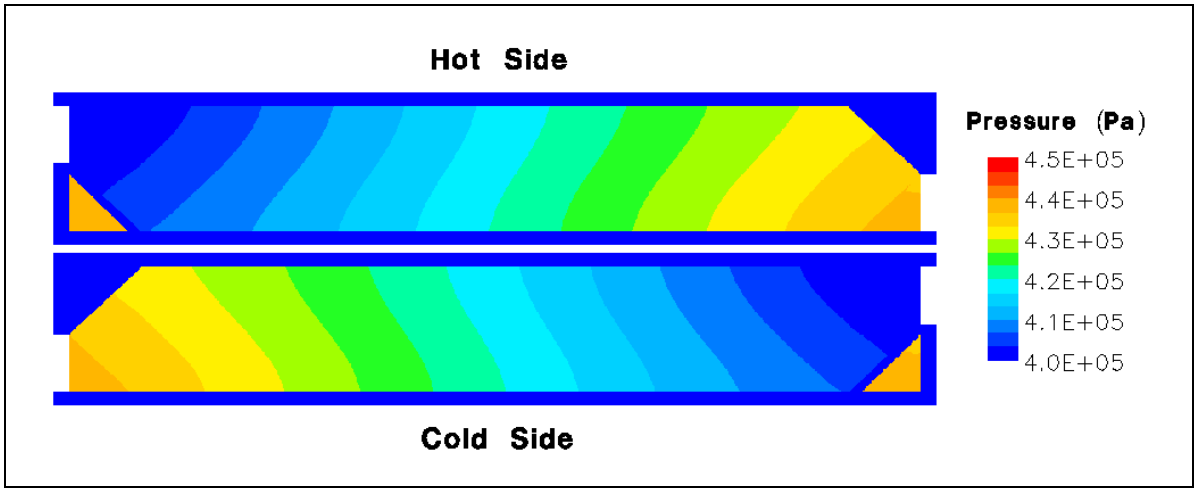


figure 32 The pressure distribution in the gas at the hot and cold side of the mock-up after 3600 seconds during the cool down transient

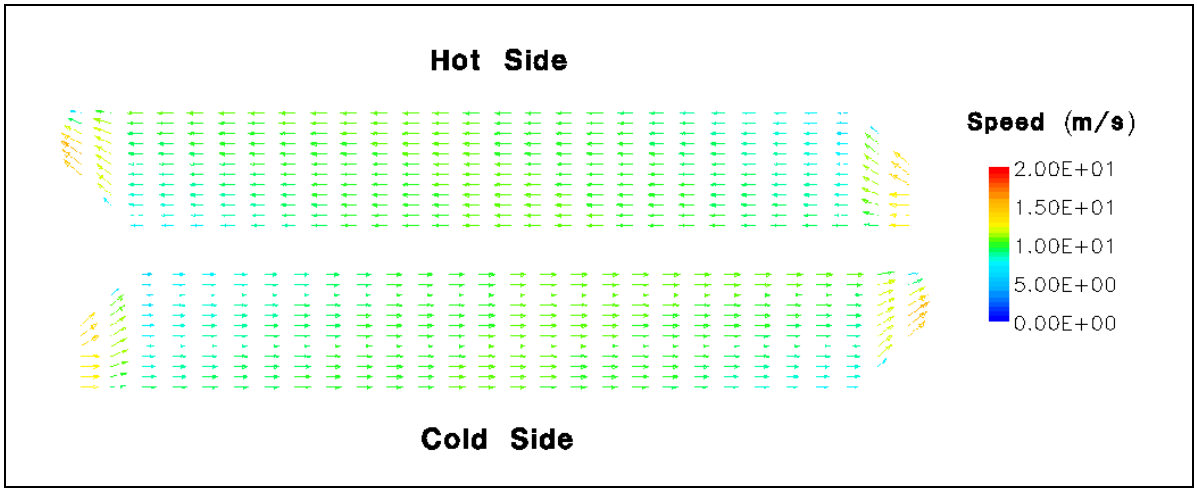


figure 33 The gas velocity distribution at the hot and cold side of the mock-up after 3600 seconds during the cool down transient

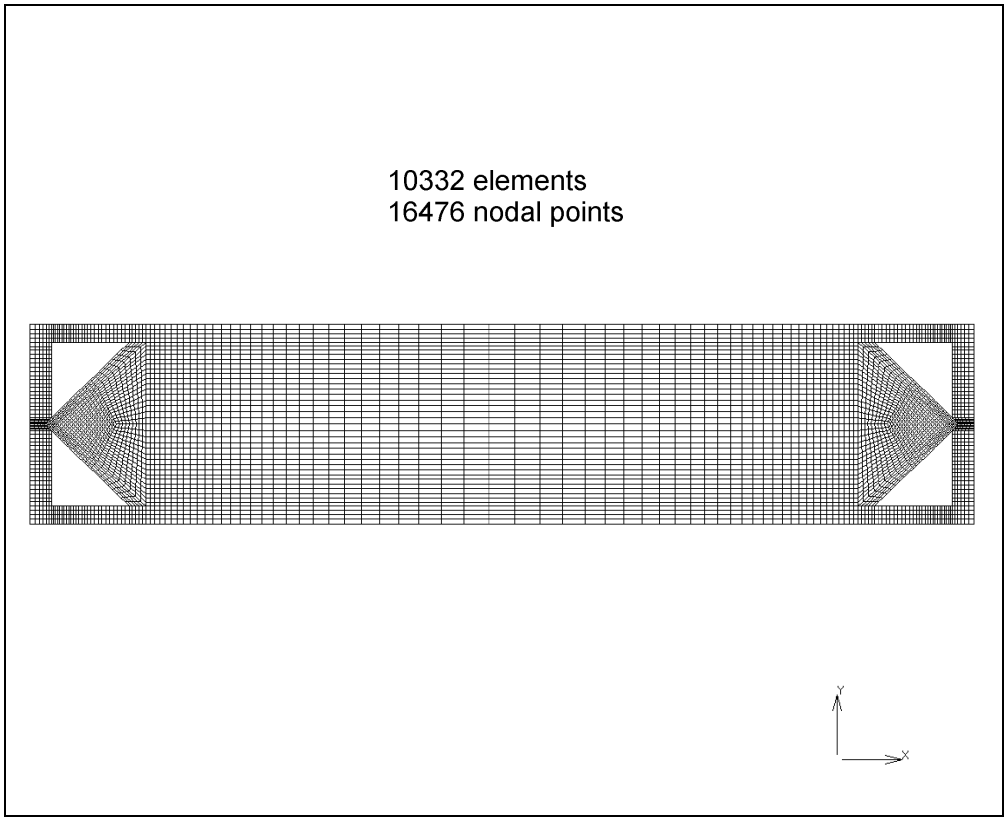


figure 34 The finite element model of the Heatric mock-up

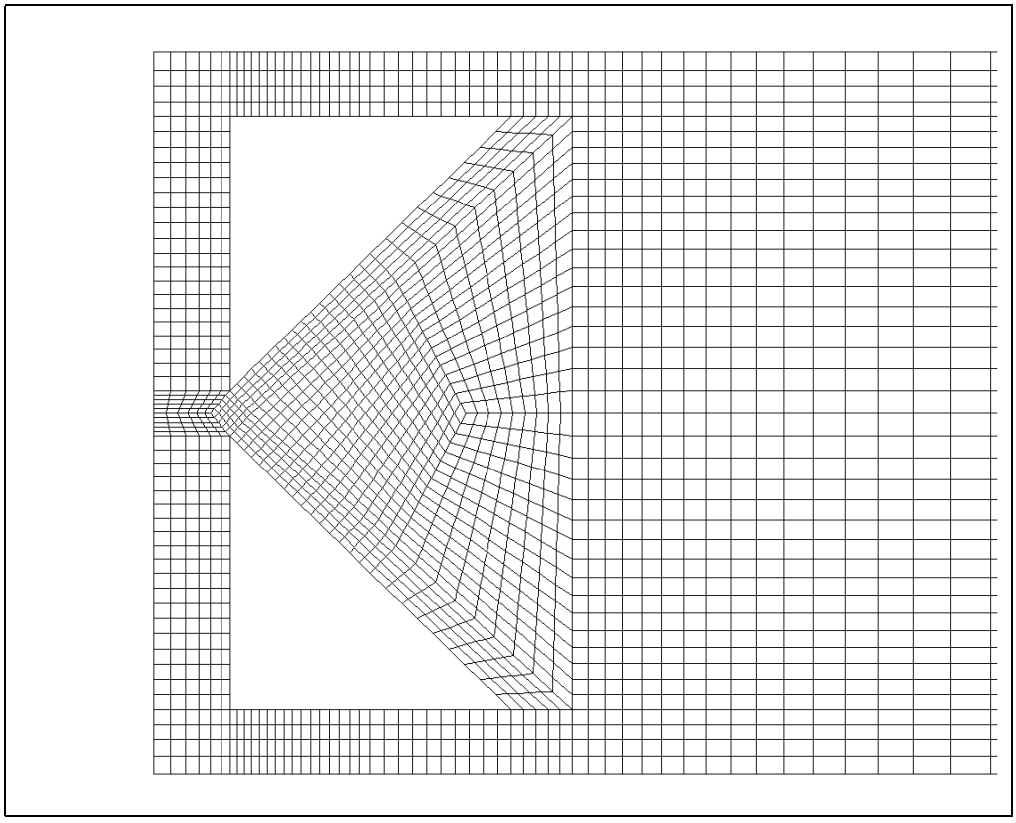


figure 35 Detailed view of the finite element model of the Heatric mock-up

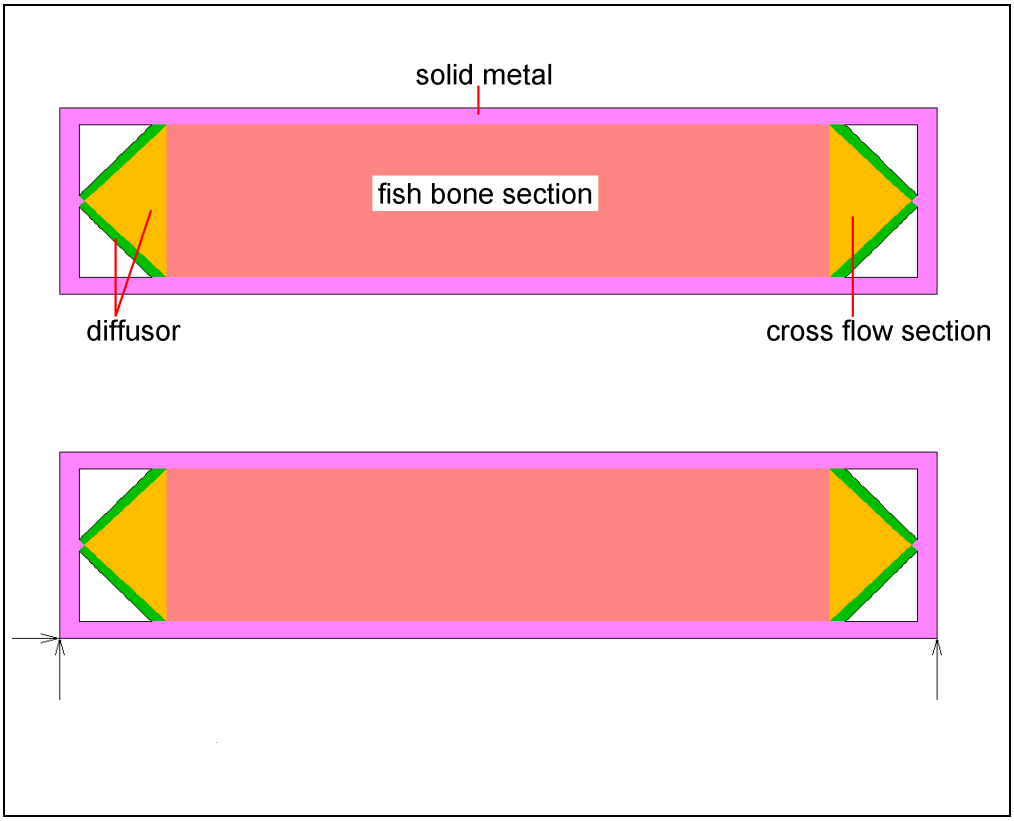


figure 36 The applied material sets and boundary conditions for the finite element model

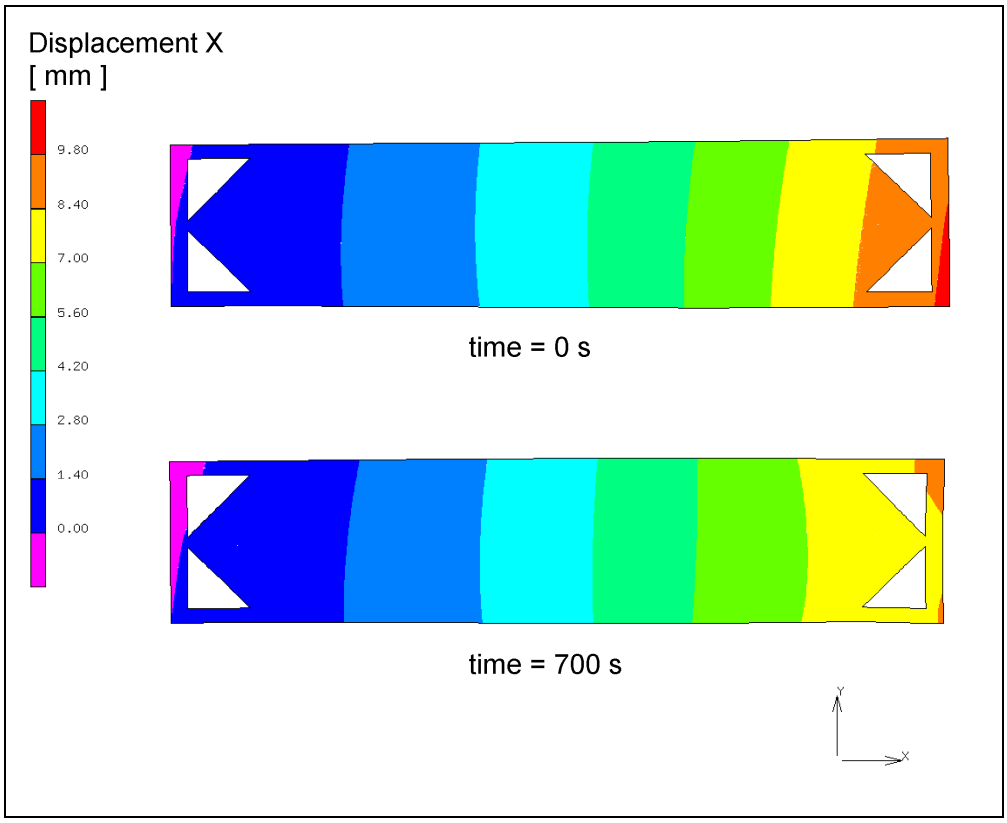


figure 37 The distribution of the axial displacement after 0 and 700 seconds during the cool down transient

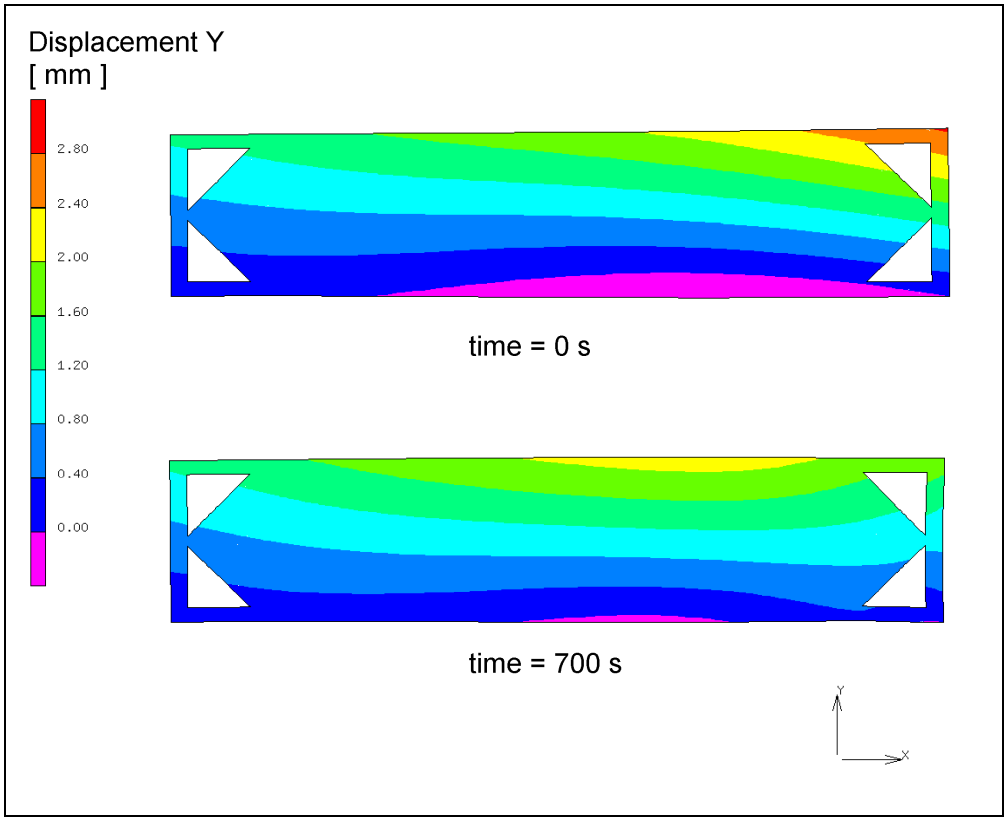


figure 38 The distribution of the displacement in thickness direction after 0 and 700 seconds during the cool down transient

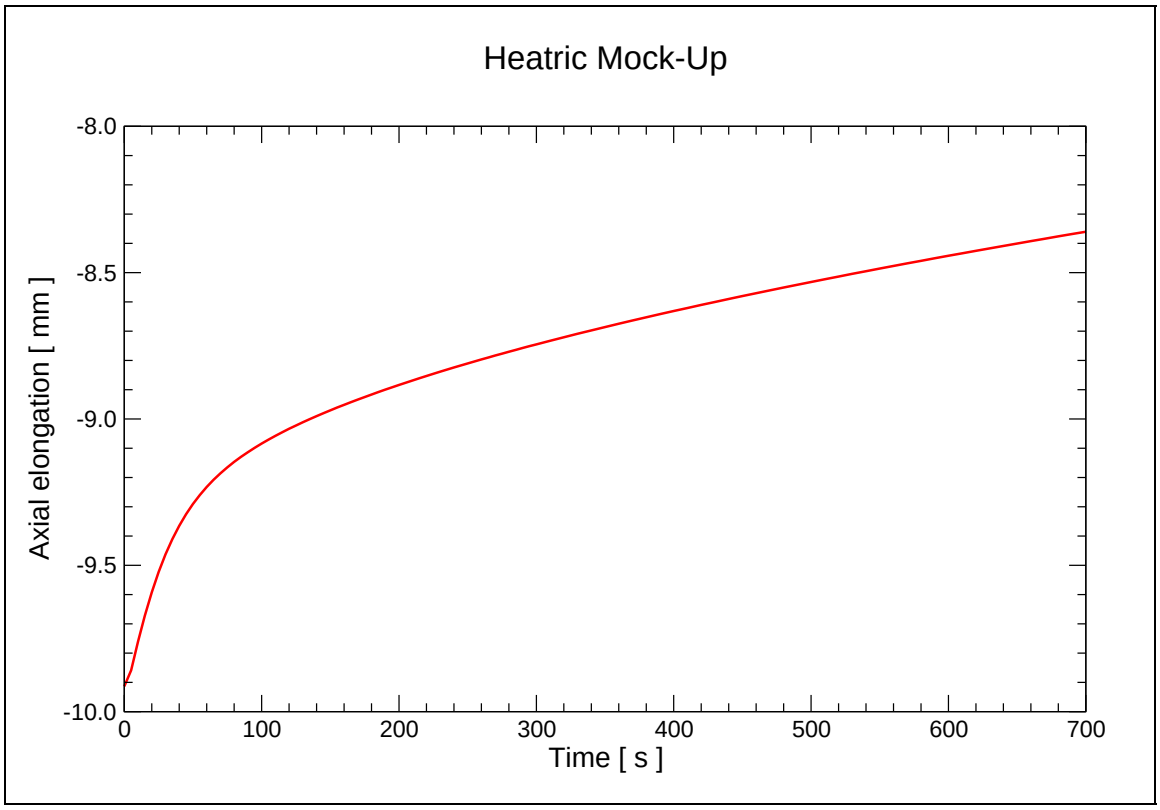


figure 39 The decrease of axial length of the mock-up as a function of time during the cool down transient

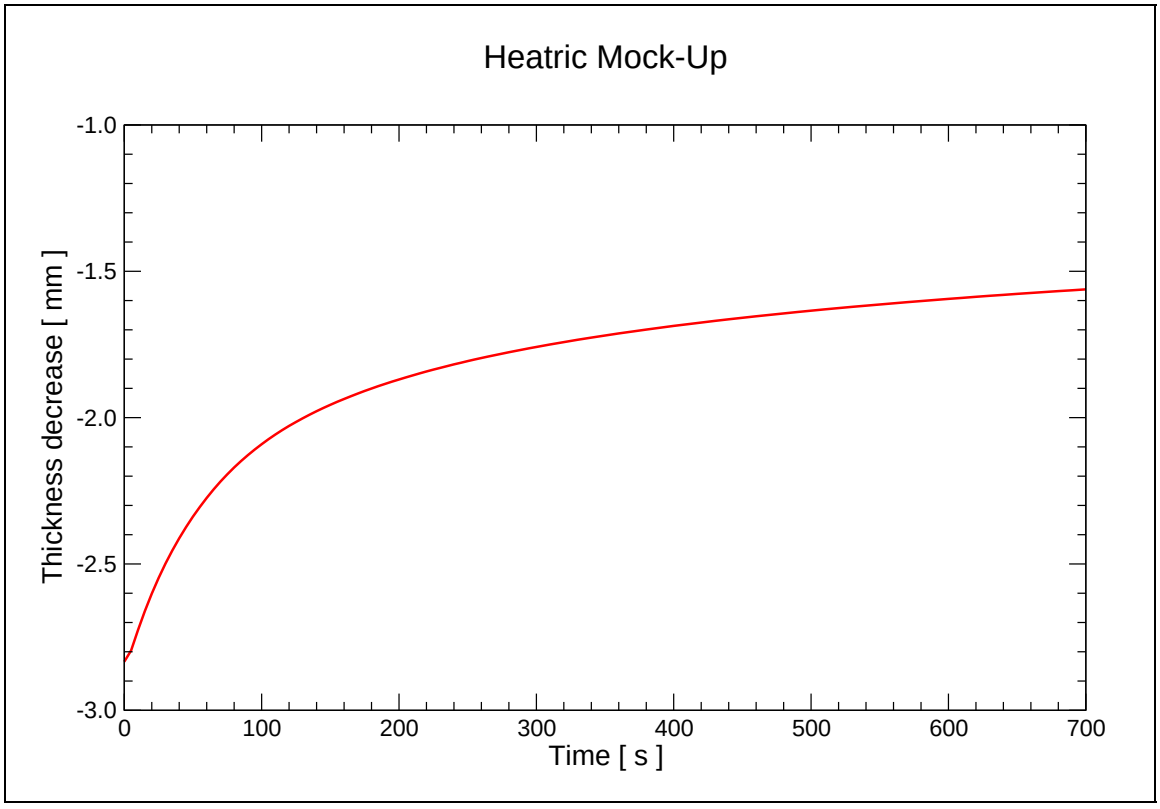


figure 40 The decrease of thickness of the mock-up as a function of time during the cool down transient

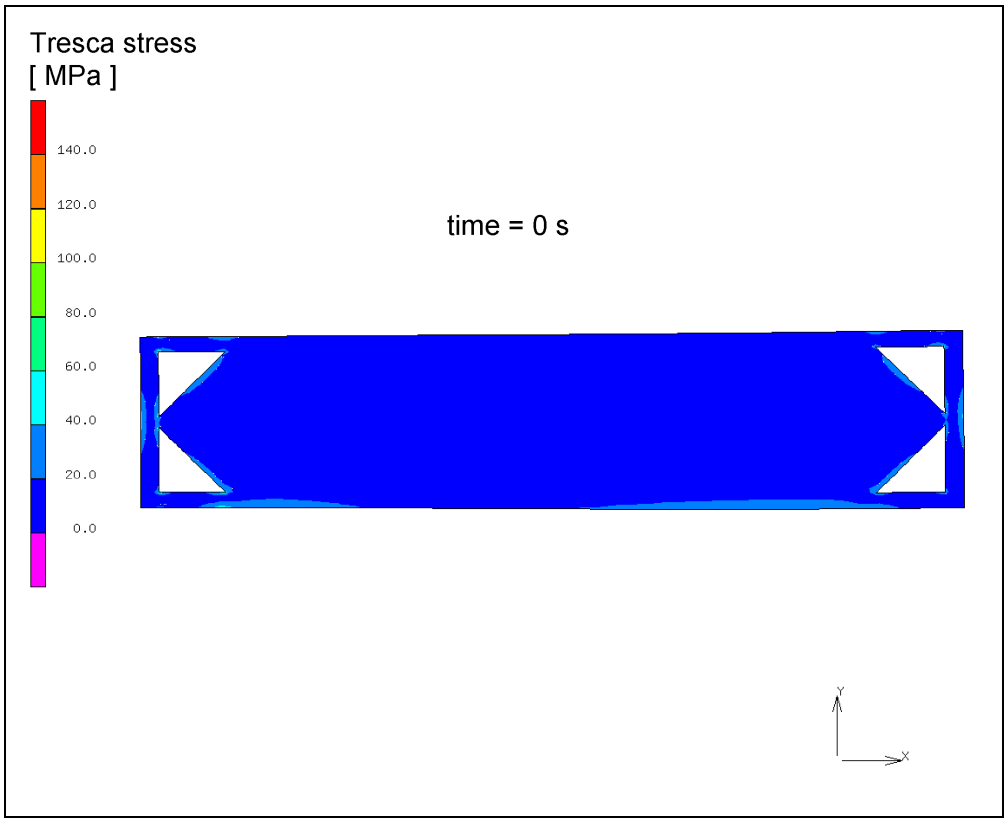


figure 41 The distribution of the Tresca stress in the mock-up after 0 seconds during the cool down transient

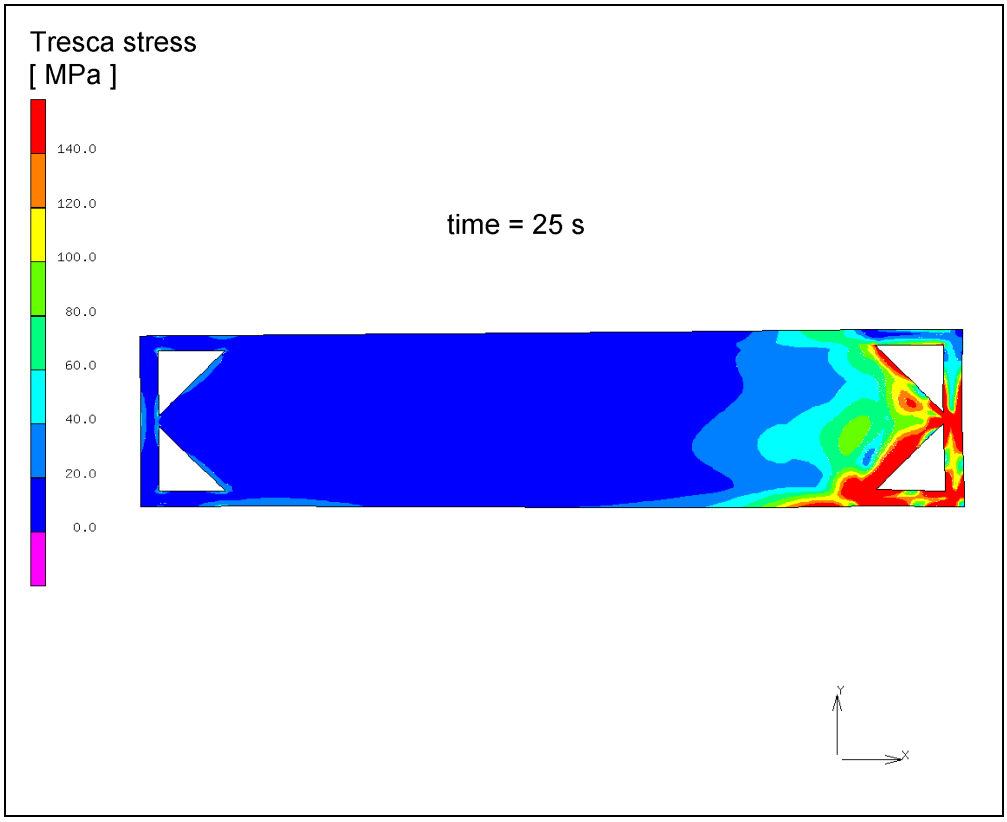


figure 42 The distribution of the Tresca stress in the mock-up after 25 seconds during the cool down transient

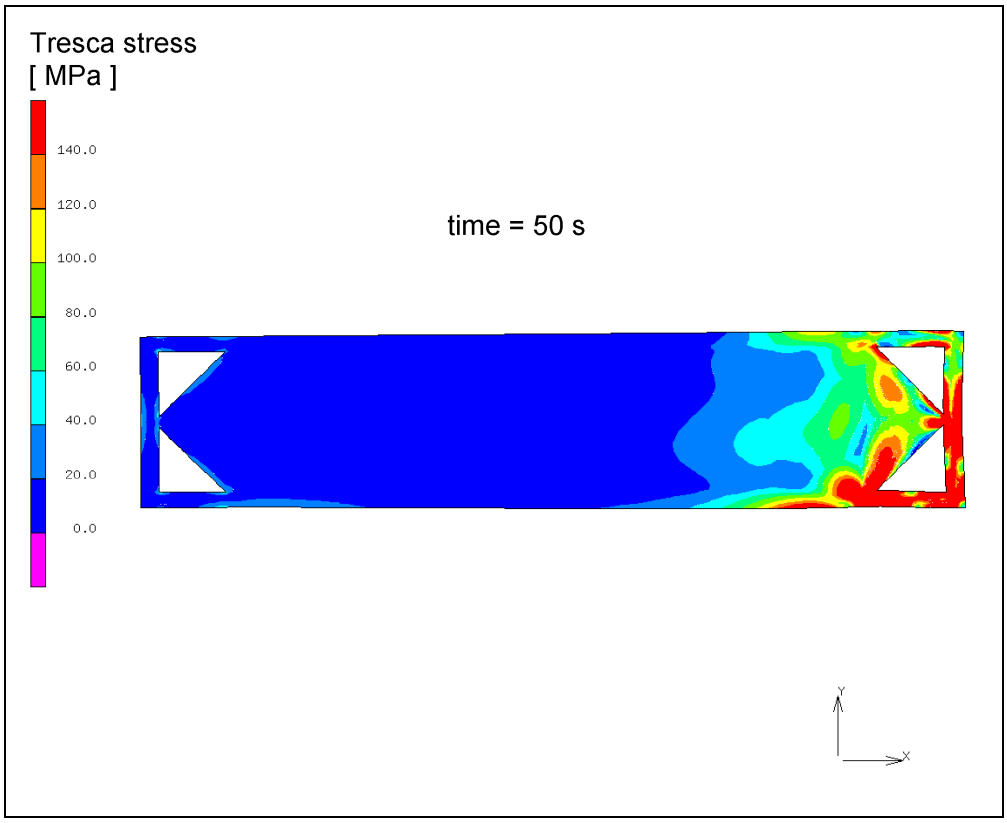


figure 43 The distribution of the Tresca stress in the mock-up after 50 seconds during the cool down transient

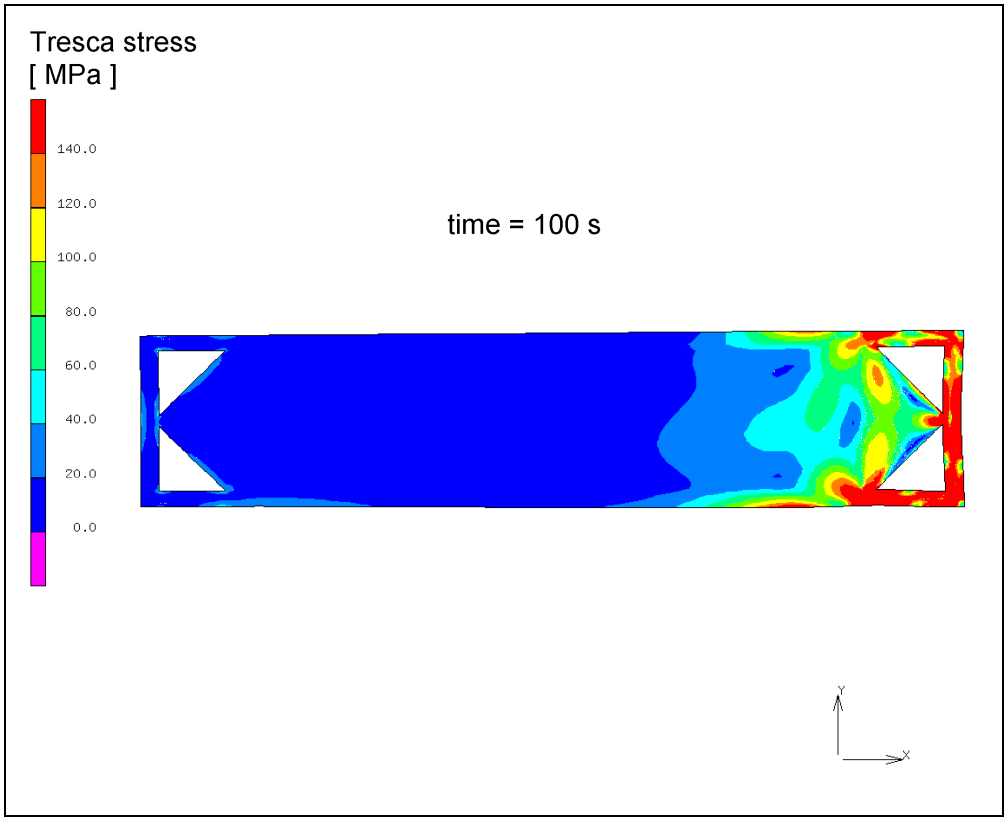


figure 44 The distribution of the Tresca stress in the mock-up after 100 seconds during the cool down transient

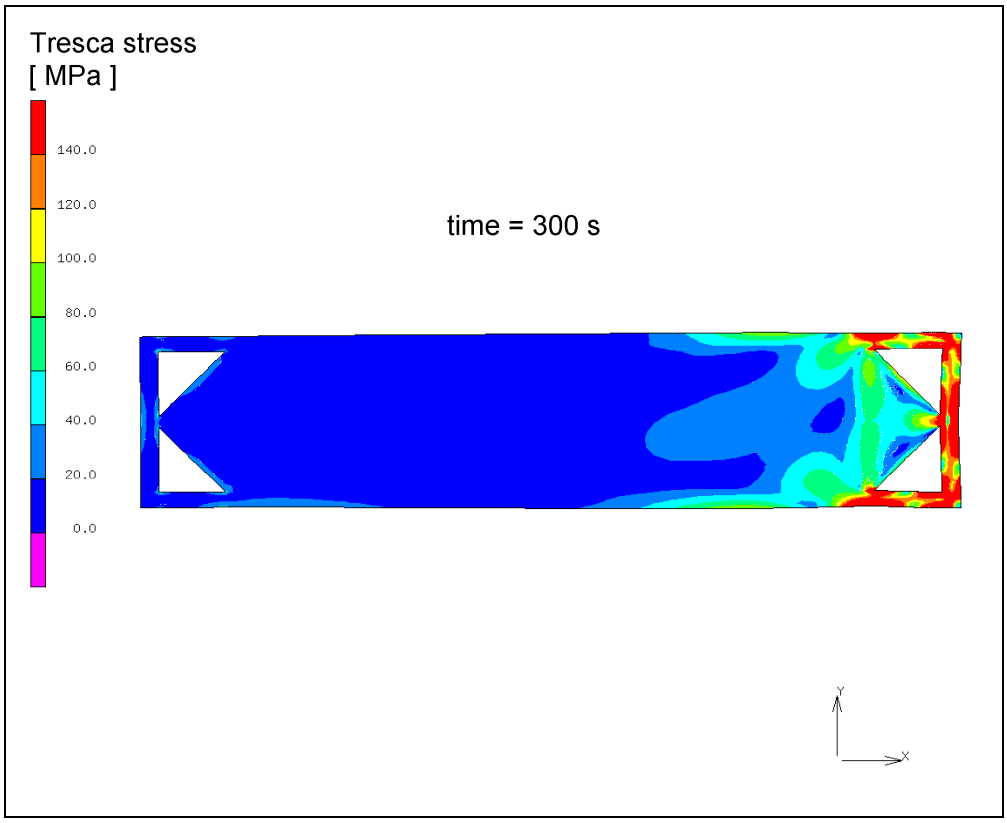


figure 45 The distribution of the Tresca stress in the mock-up after 300 seconds during the cool down transient

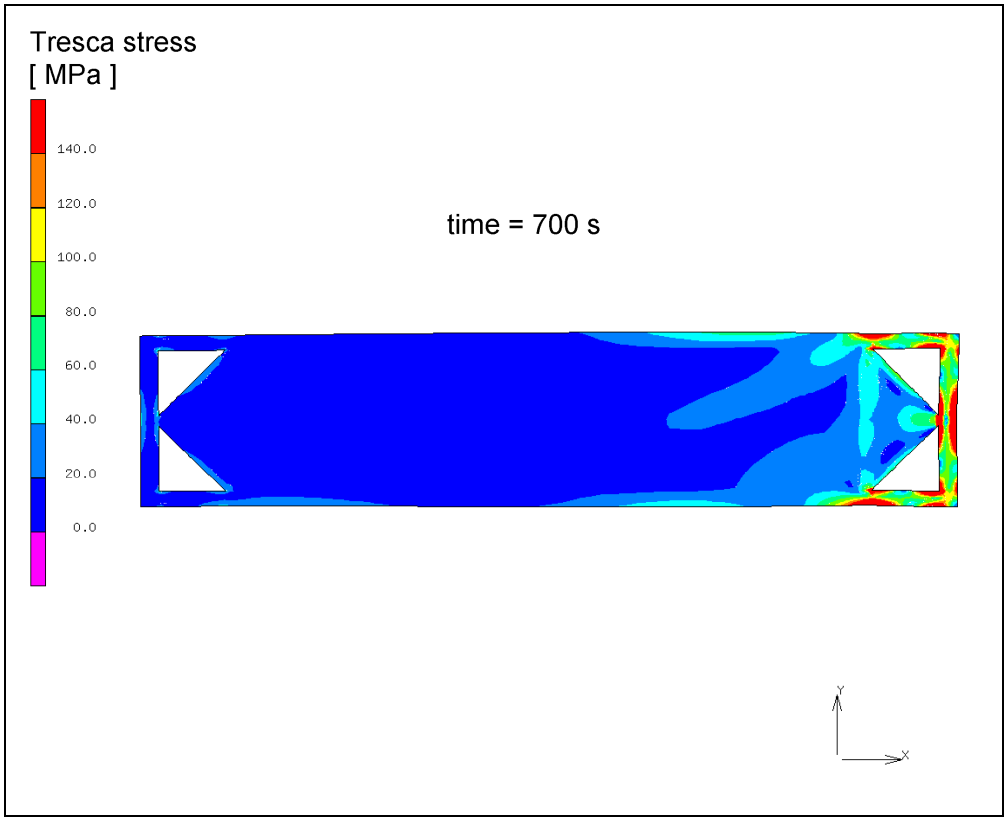


figure 46 The distribution of the Tresca stress in the mock-up after 700 seconds during the cool down transient

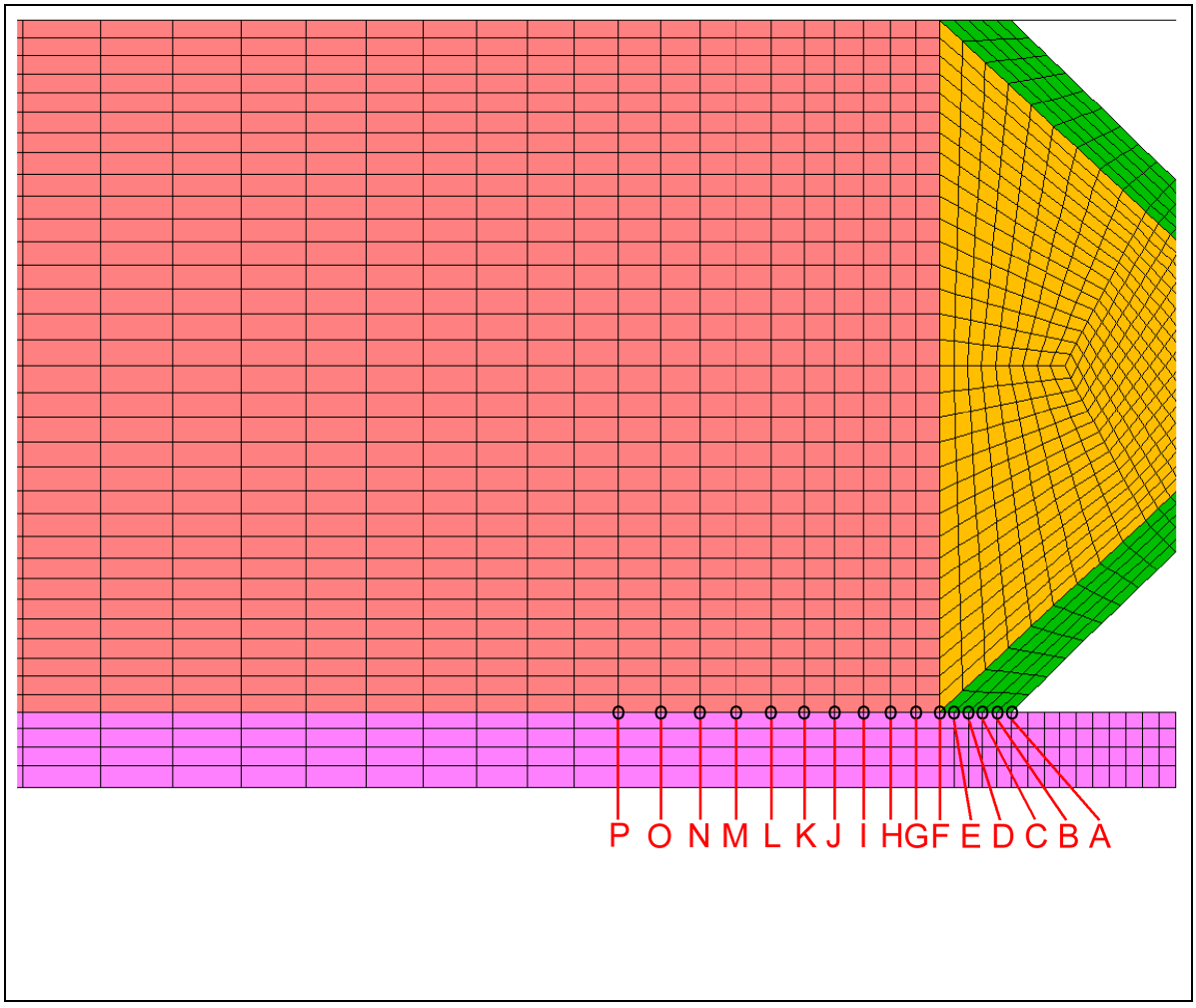


figure 47 The most critical positions with respect to fatigue damage in the Heatric mock-up

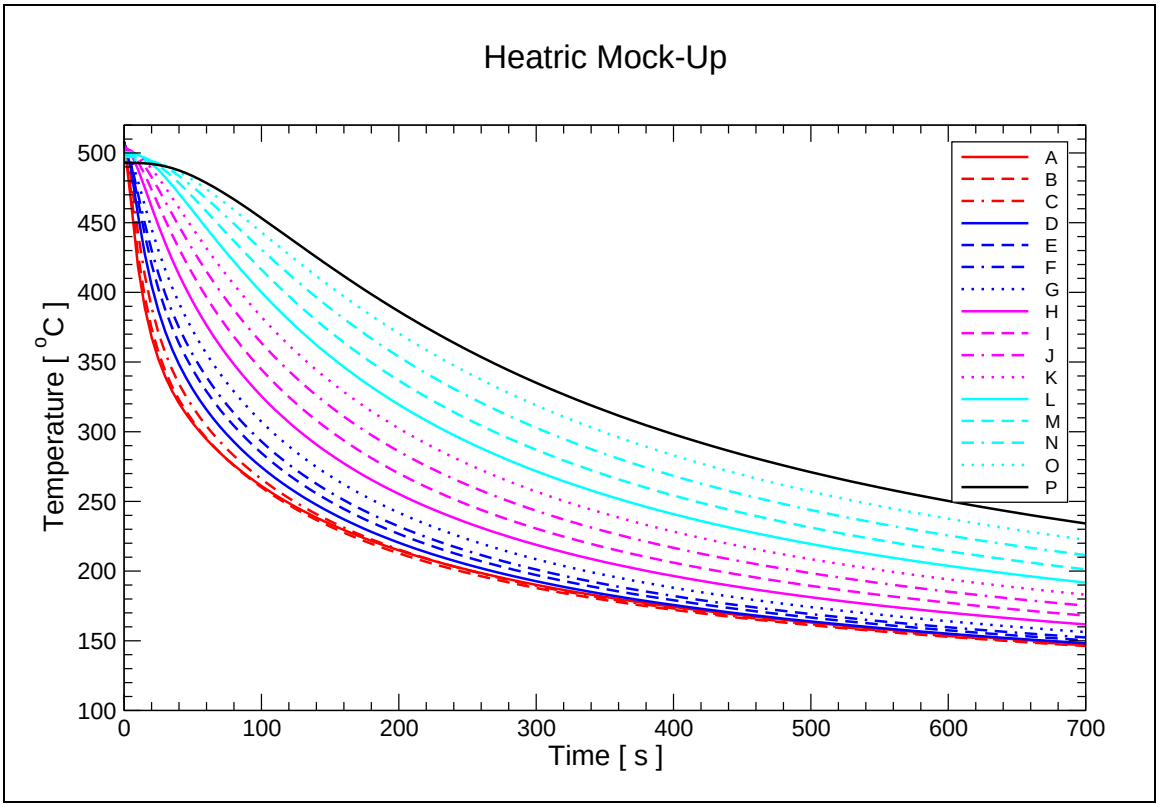


figure 48 The temperature in the critical positions as a function of time

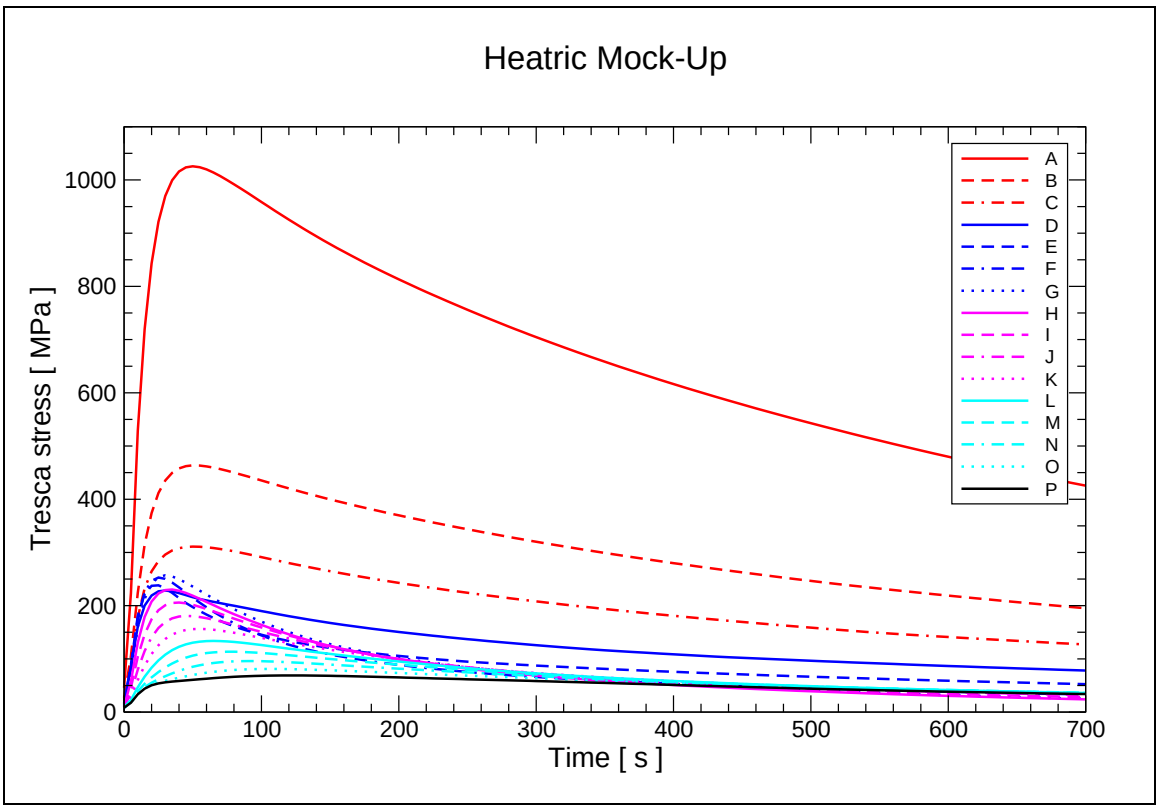


figure 49 The Tresca stress in the critical positions as a function of time

Appendix A

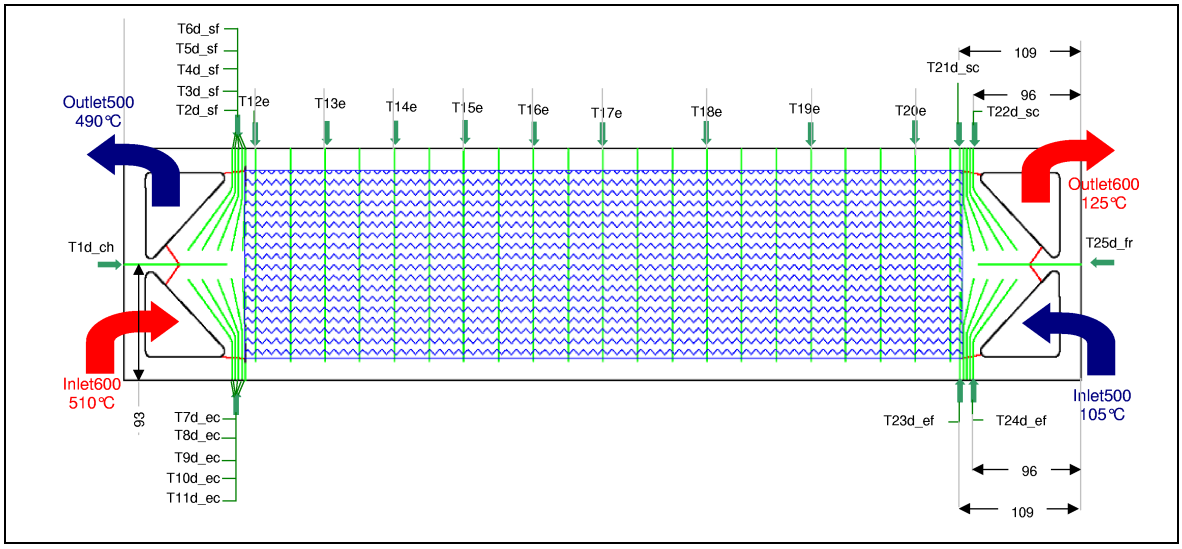


figure A.1 The positions of all thermocouples

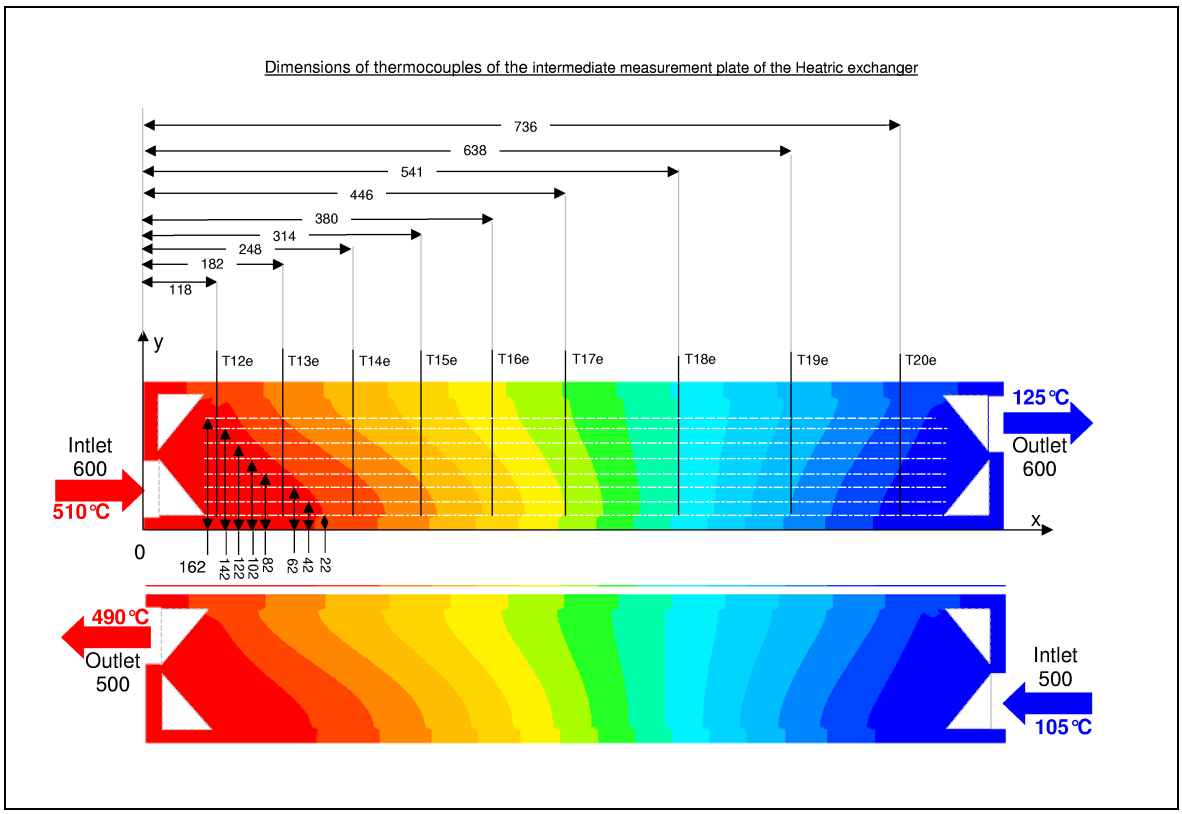


figure A.2 The possible positions of the thermocouples T12e up to T20e

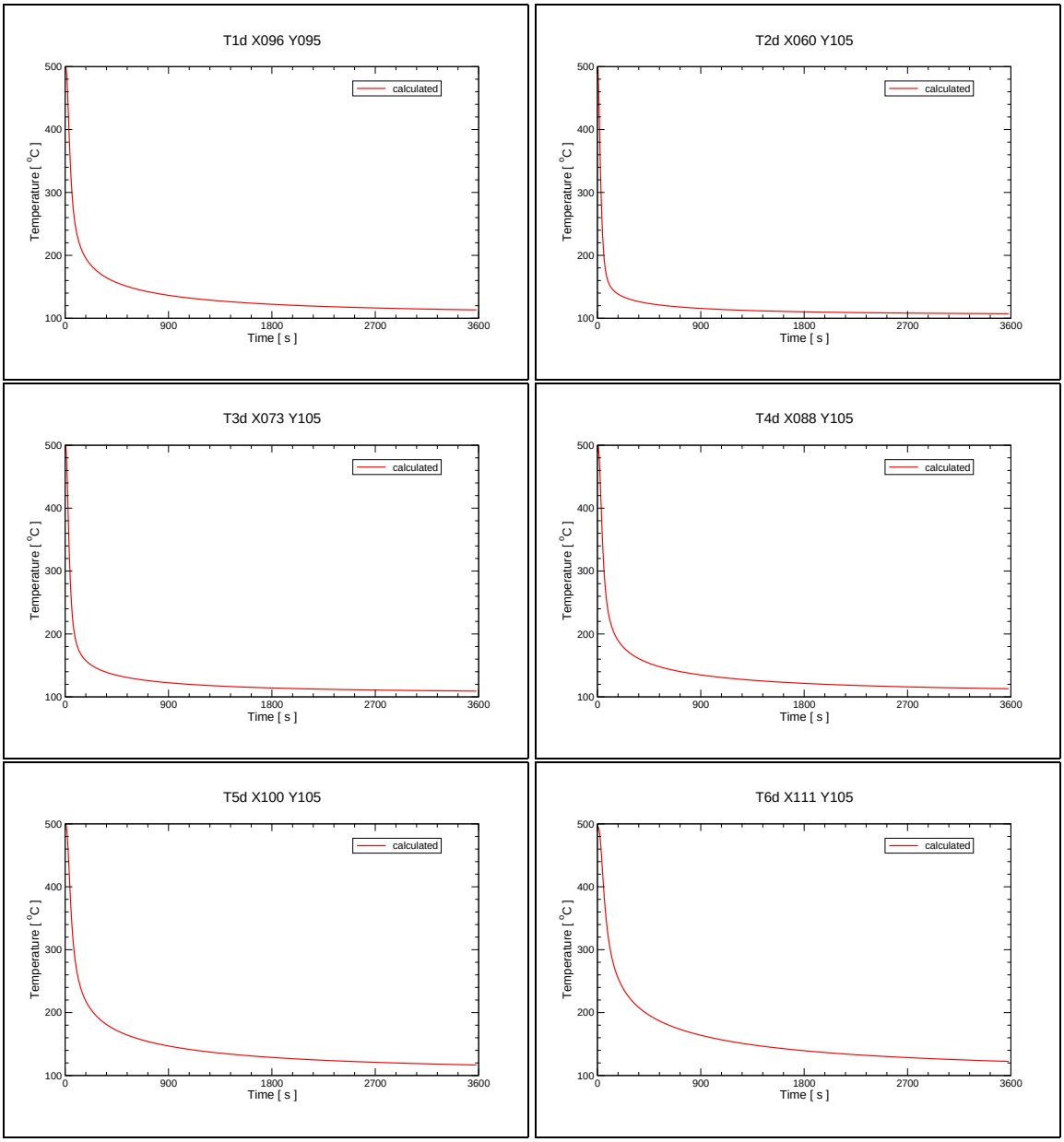


figure A.3 The predicted temperature as a function of time for thermocouples T1d untill T6d

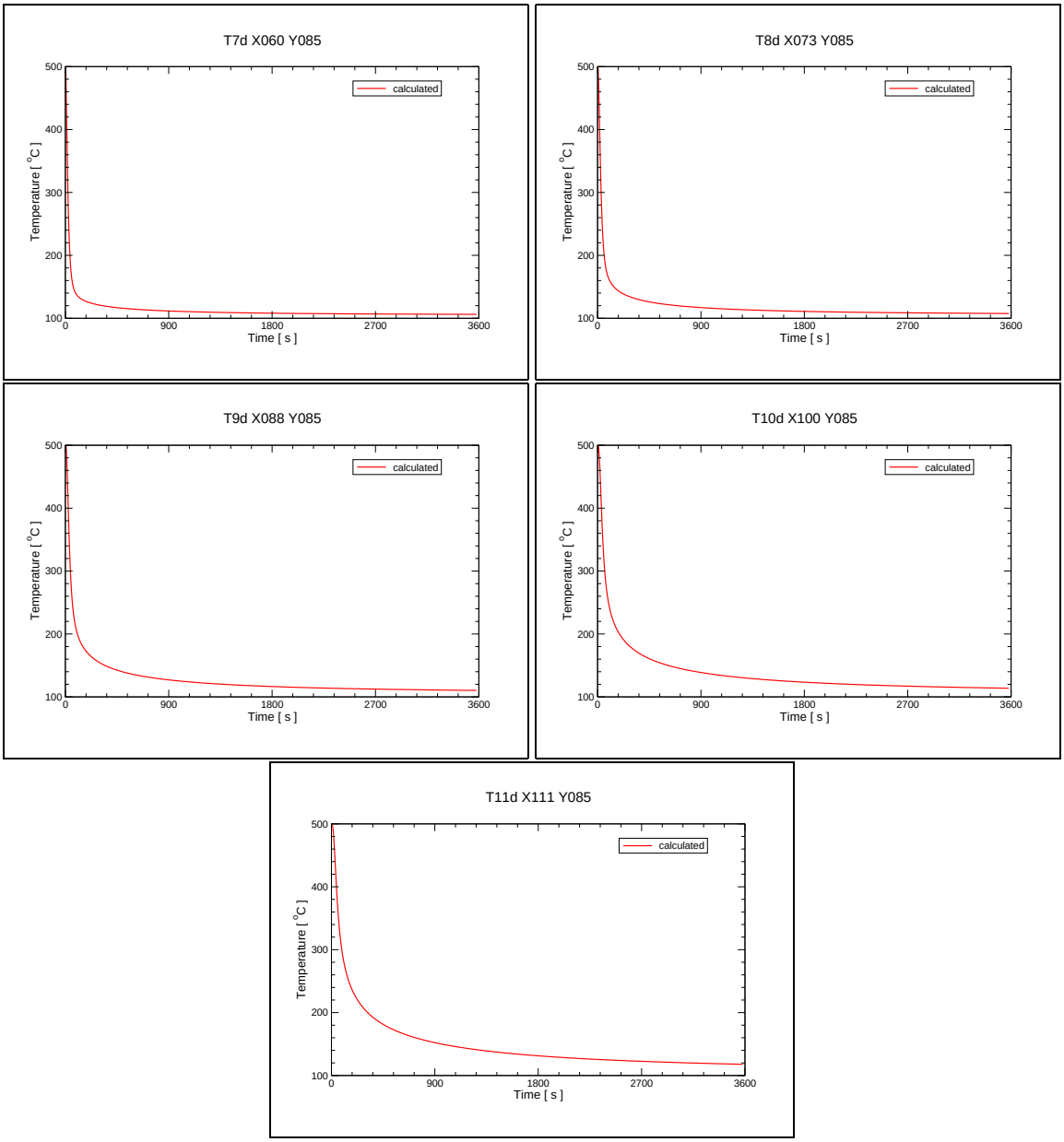


figure A.4 The predicted temperature as a function of time for thermocouples T7d_ec untill T11d_ec

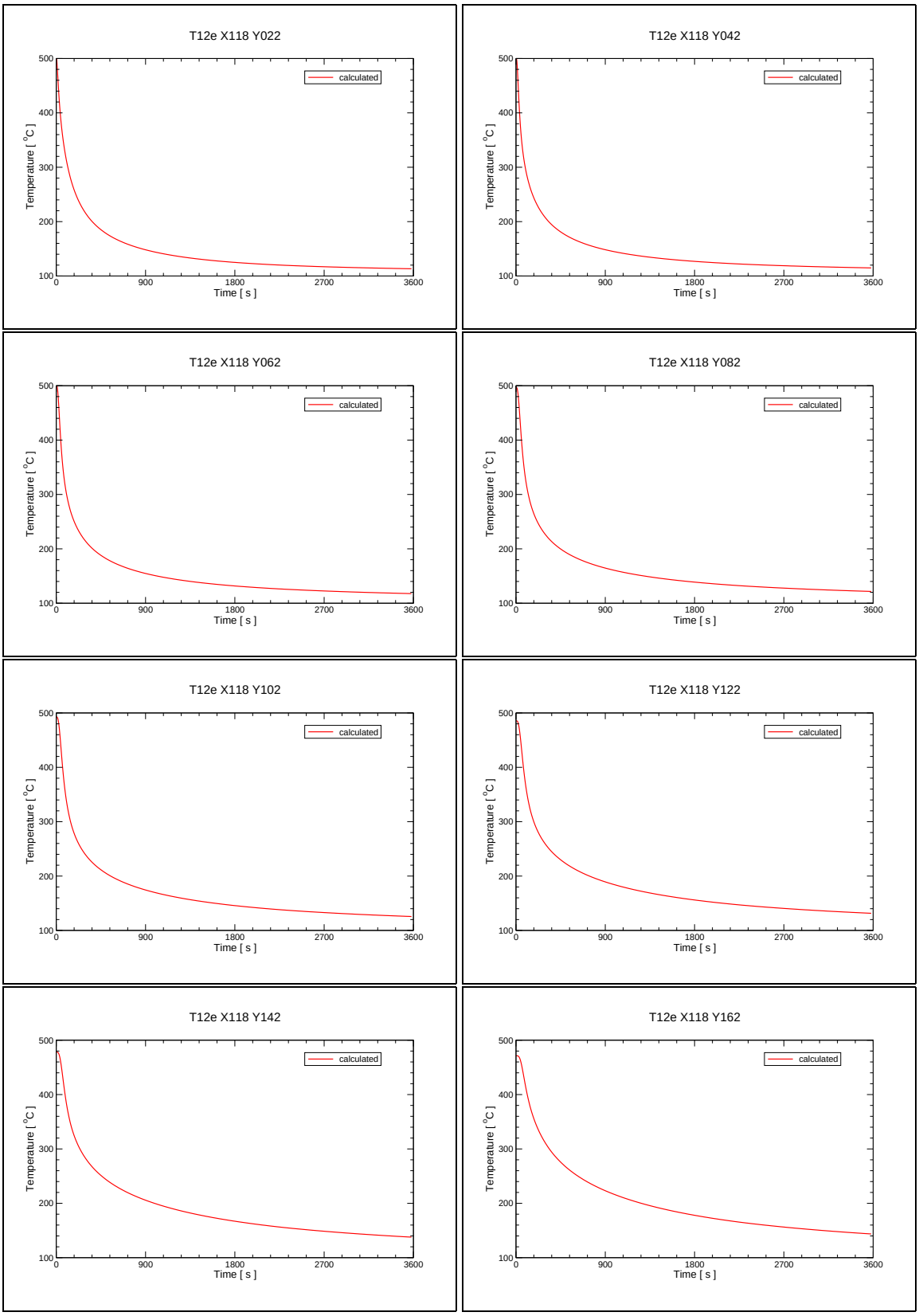


figure A.5 The predicted temperature as a function of time for thermocouple T12e at different levels

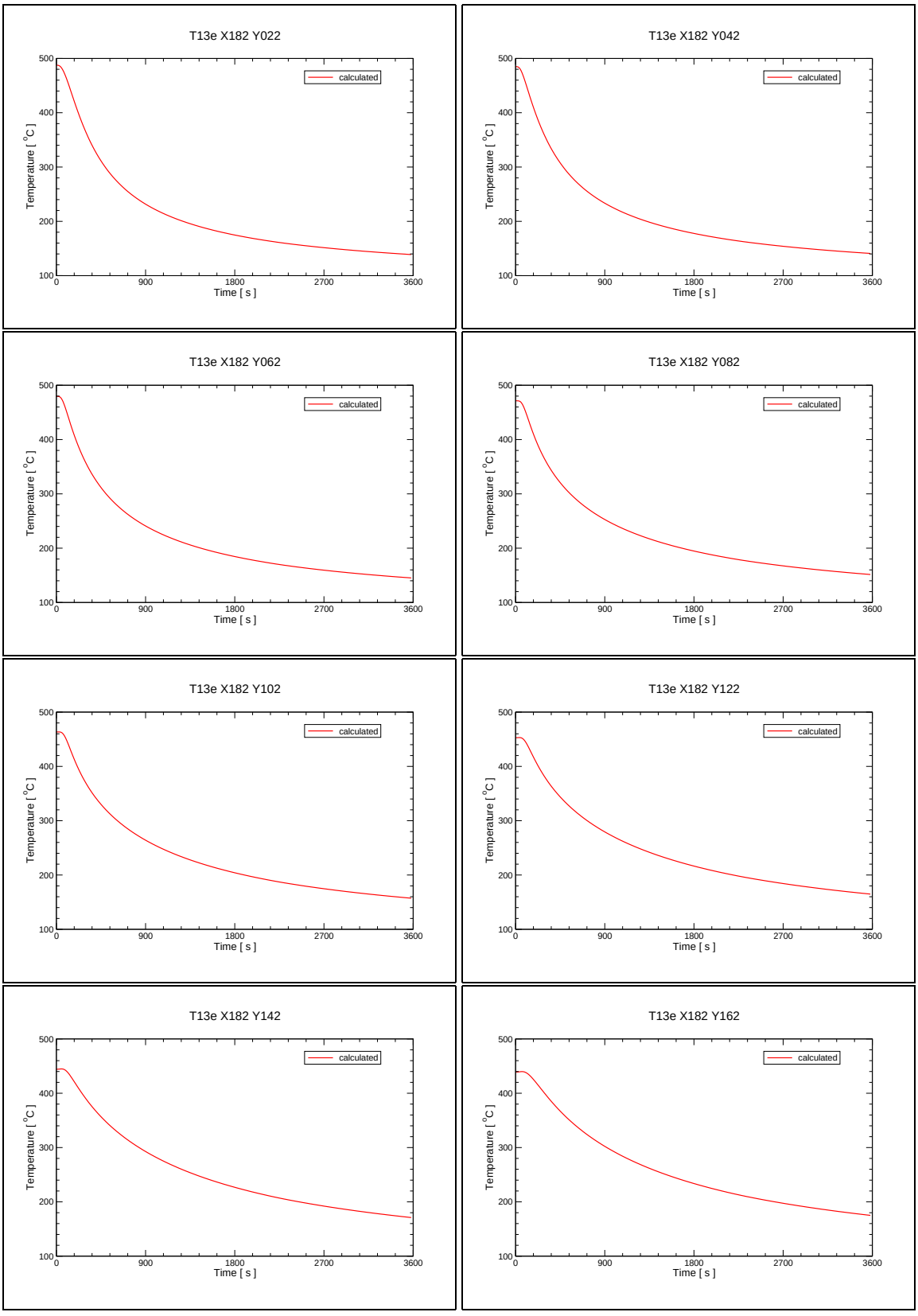


figure A.6 The predicted temperature as a function of time for thermocouple T13e at different levels

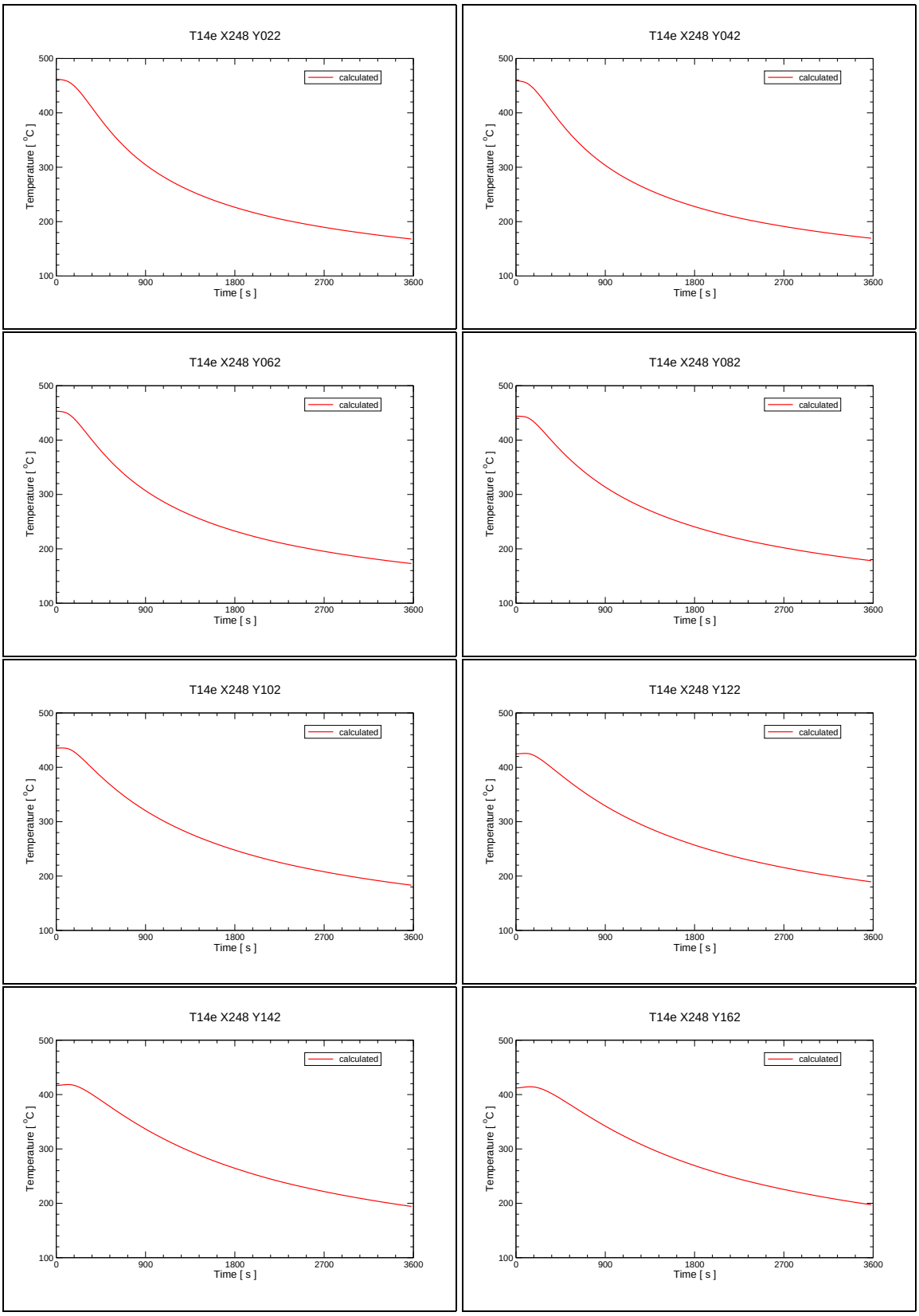


figure A.7 The predicted temperature as a function of time for thermocouple T14e at different levels

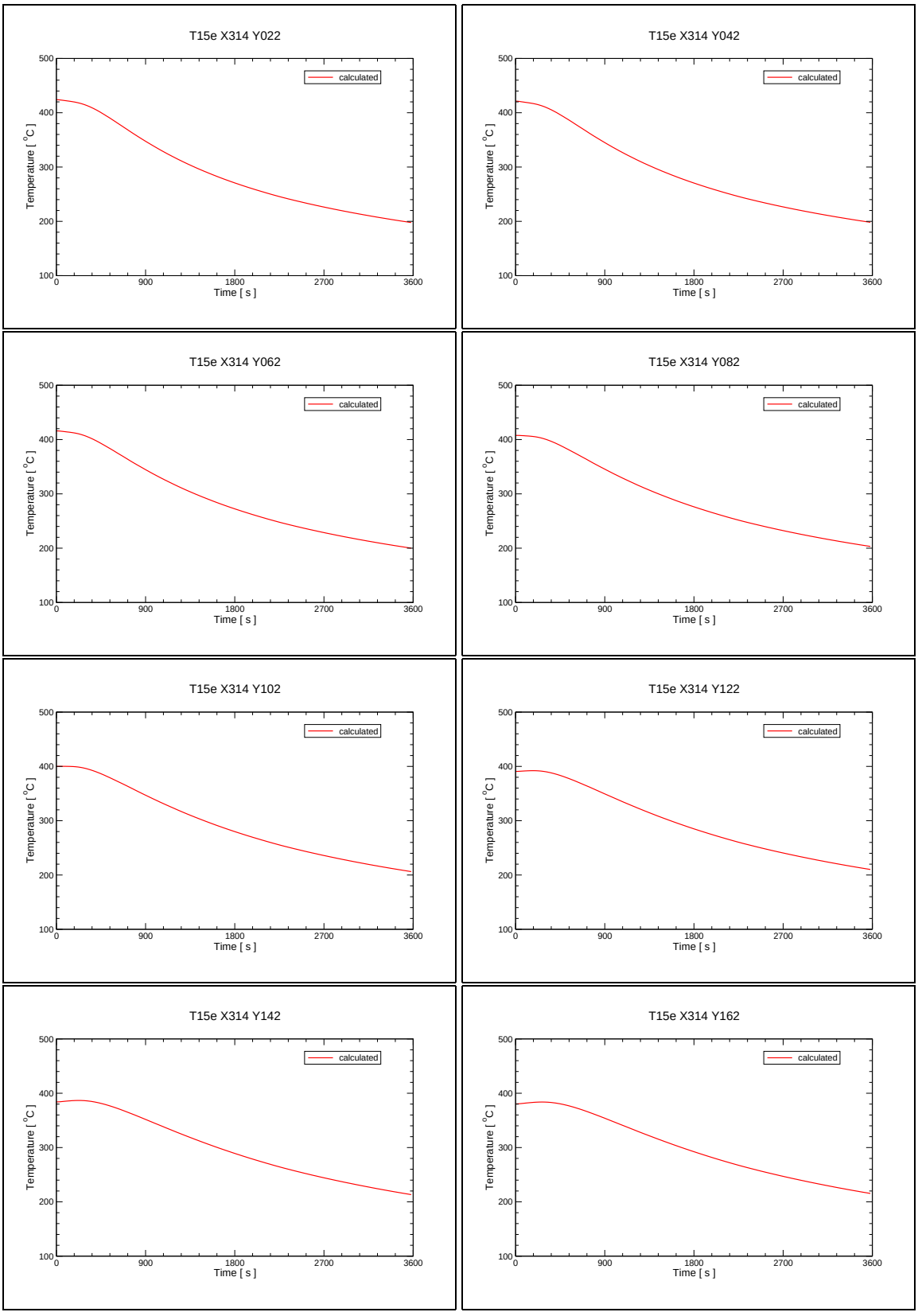


figure A.8 The predicted temperature as a function of time for thermocouple T15e at different levels

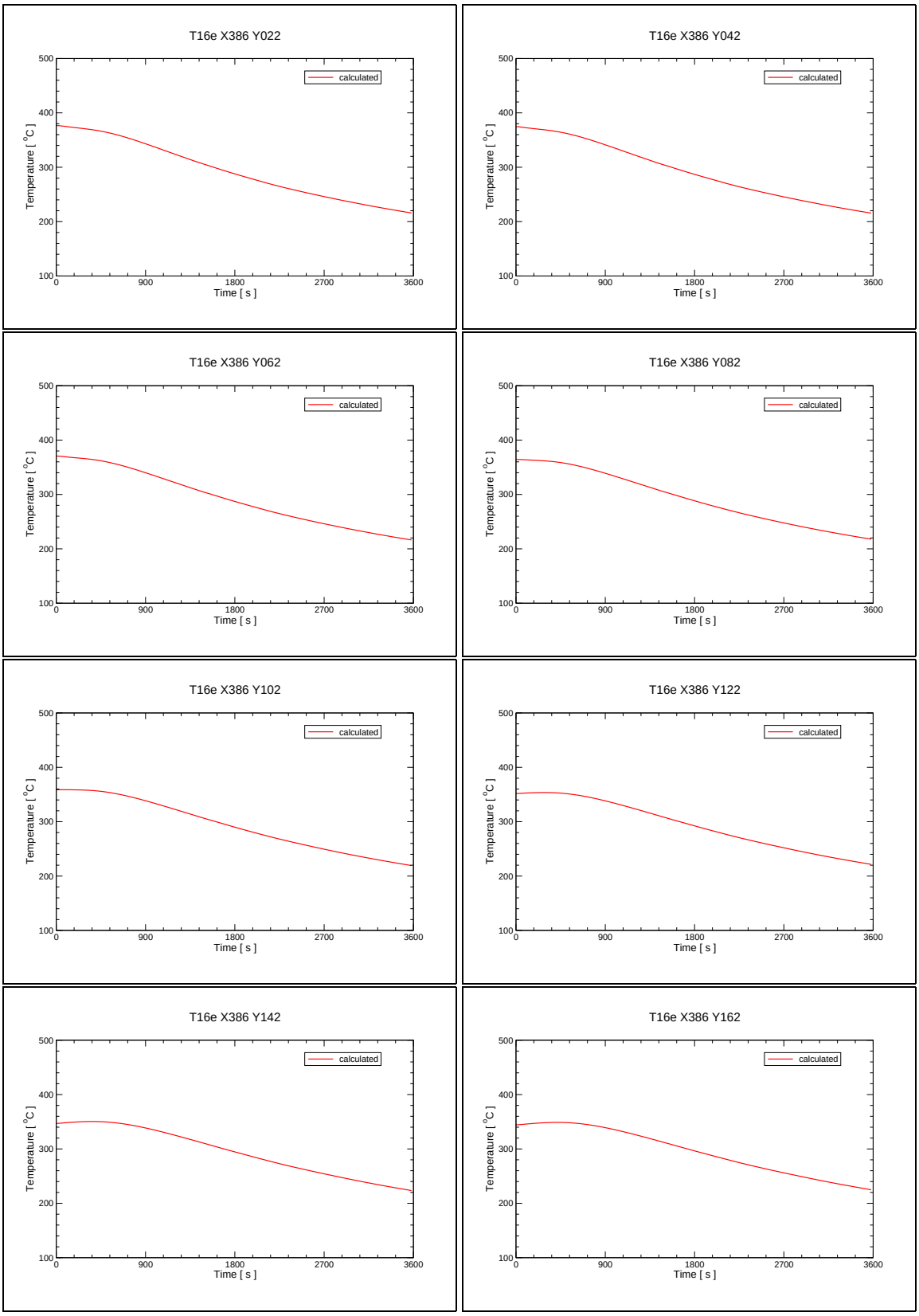


figure A.9 The predicted temperature as a function of time for thermocouple T16e at different levels

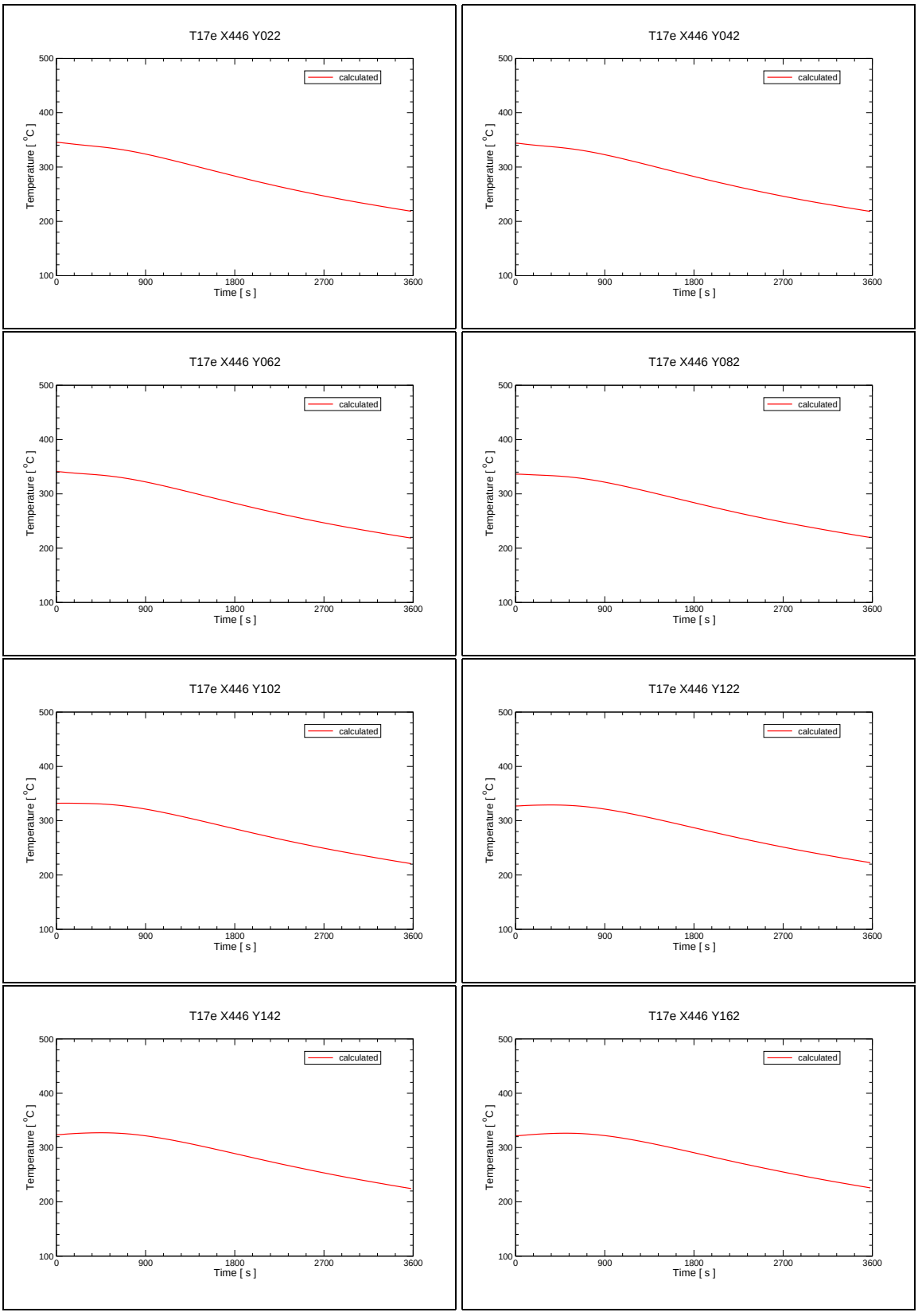


figure A.10 The predicted temperature as a function of time for thermocouple T17e at different levels

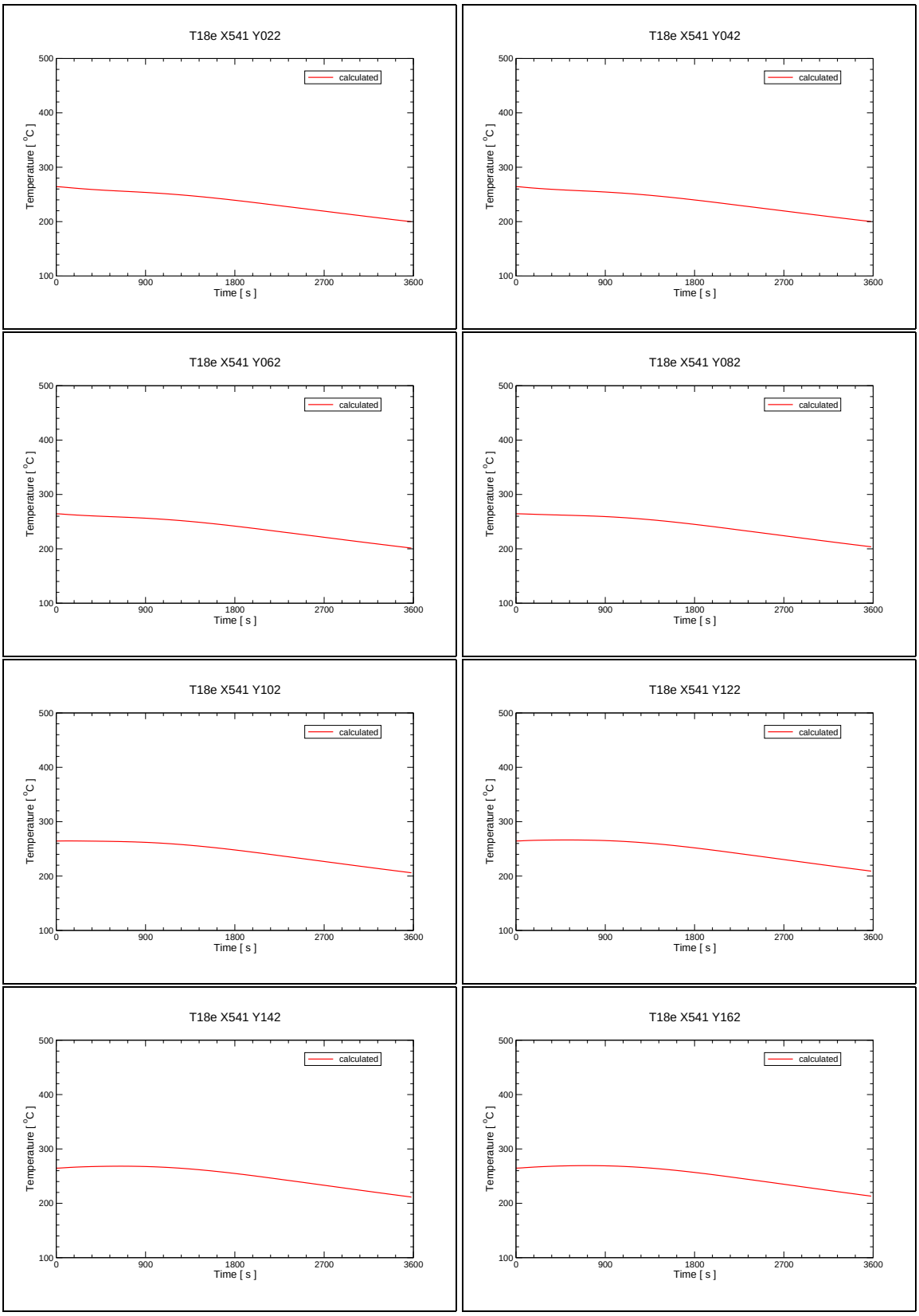


figure A.11 The predicted temperature as a function of time for thermocouple T18e at different levels

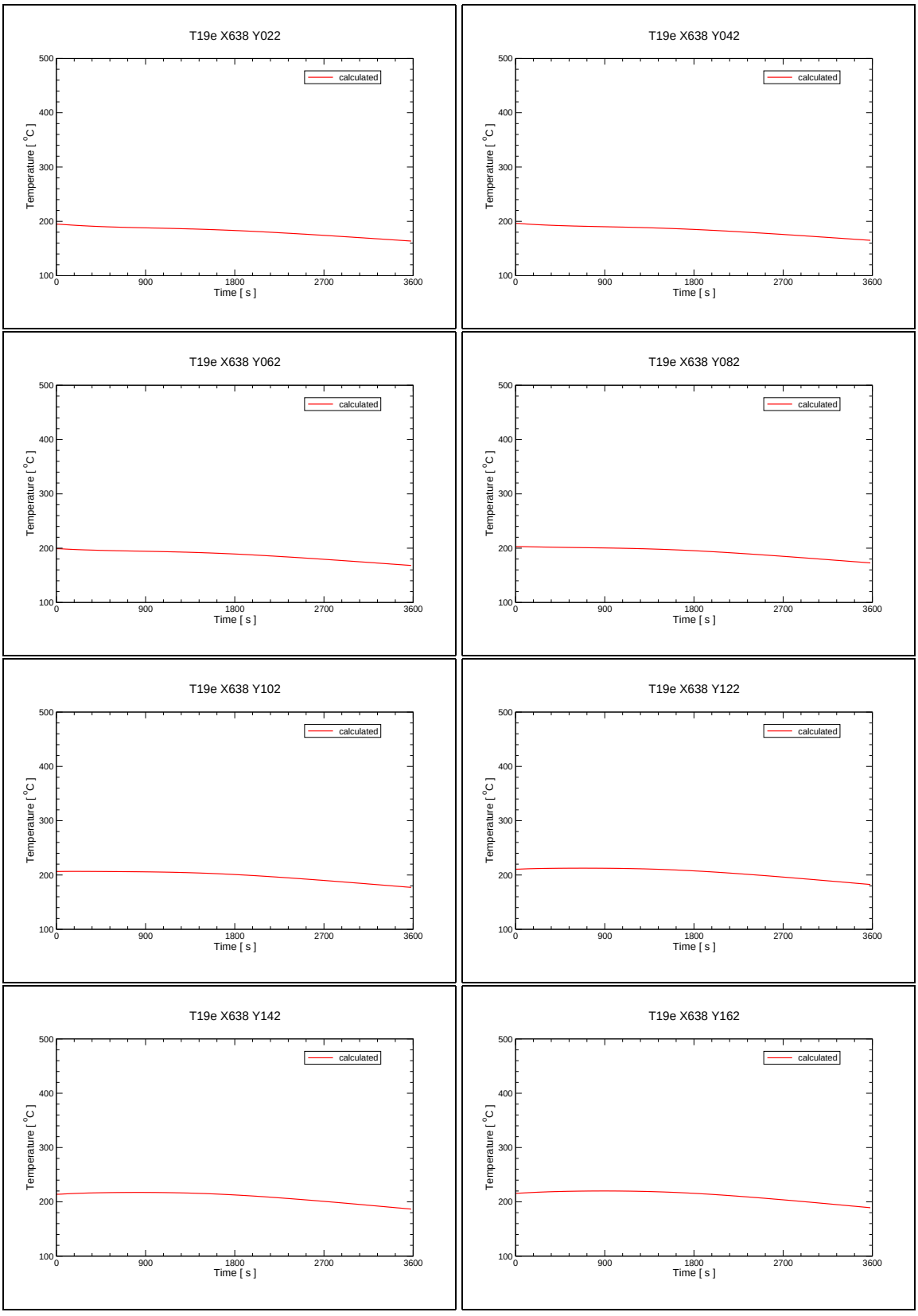


figure A.12 The predicted temperature as a function of time for thermocouple T19e at different levels

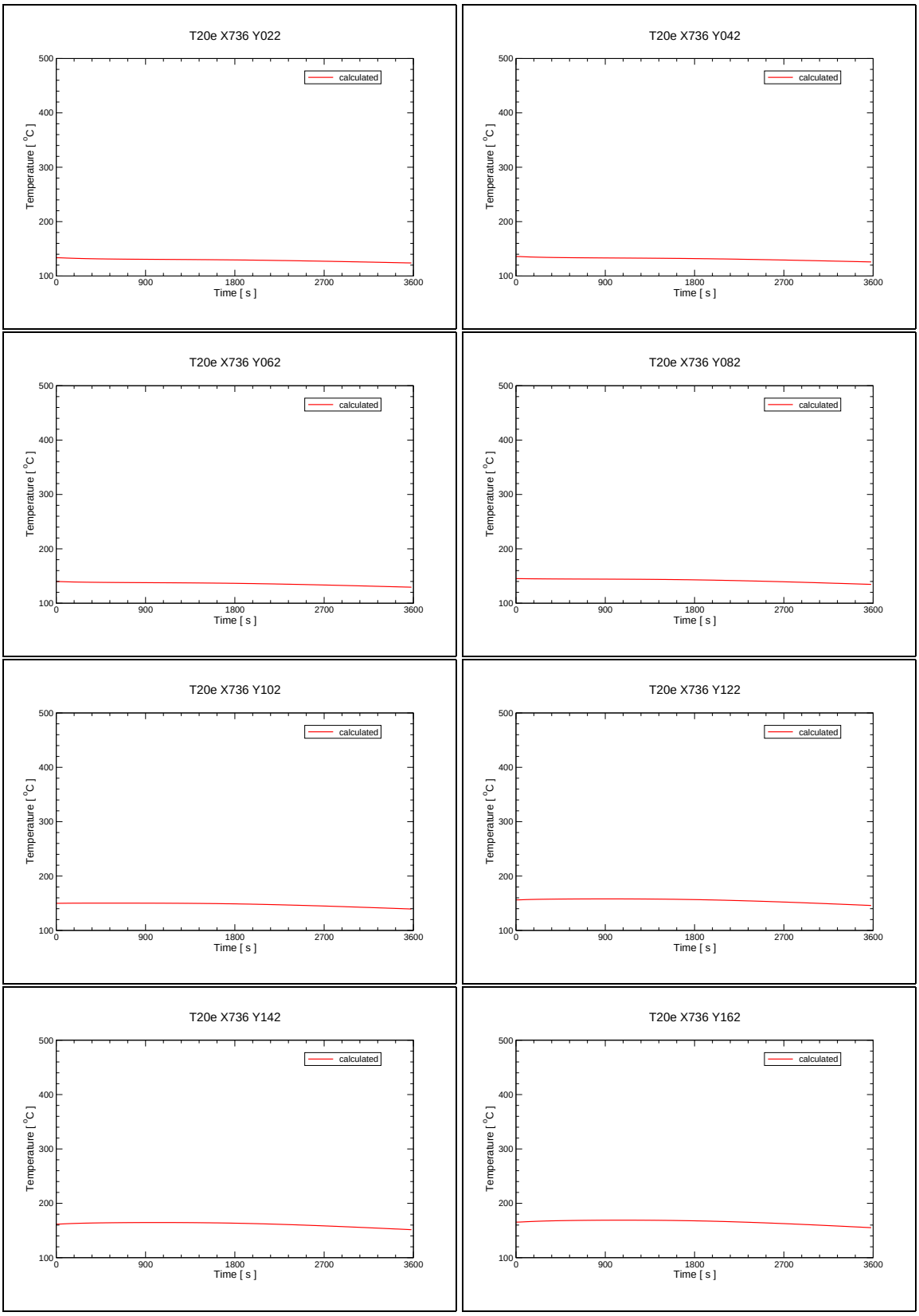


figure A.13 The predicted temperature as a function of time for thermocouple T20e at different levels

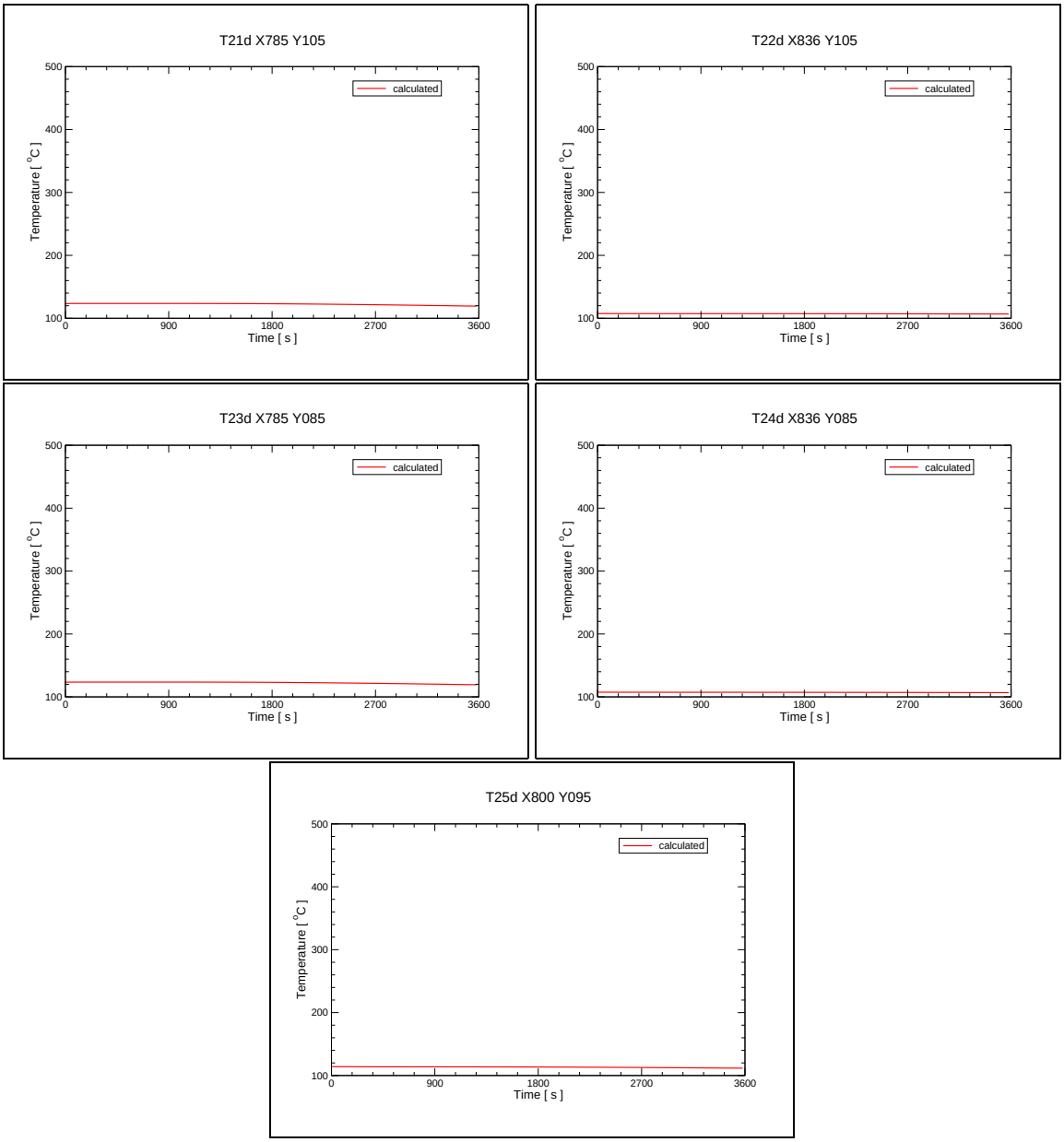


figure A.14 The predicted temperature as a function of time for thermocouples T21d untill T25d